Checkered Landscapes: Quantifying Dominant Control on Nitrogen Legacies and Time Lags along the River Continuum

by

Yuhe Liu

A thesis
presented to the University of Waterloo
in fulfilment of the
thesis requirement for the degree of
Master of Applied Science
in
Civil Engineering (Water)

Waterloo, Ontario, Canada, 2020

Author's Declaration

This thesis consists of material all of which I authored or co-authored: see Statement of contributions included in the thesis. This is a true copy of the thesis, including any required final revisions, as accepted by my examiners.

I understand that my thesis may be made electronically available to the public.

Statement of contributions

I would like to acknowledge my co-authors Drs. Kimberly Van Meter and Nandita Basu who contributed to the research described in this thesis.

Abstract

In agricultural watersheds across the world, decades of commercial fertilizer application and intensive livestock production have led to elevated stream nutrient levels and problems of eutrophication in both inland and coastal waters. Despite widespread implementation of a range of strategies to reduce nutrient export to receiving water bodies, expected improvements in water quality have often not been observed. It is increasingly understood that long time lags to seeing reductions in stream nutrient concentrations can result from the existence of legacy nutrient stores within the landscape. However, it is less understood how spatial heterogeneity in legacy nutrient dynamics might allow us to target implementation of appropriate management practices.

In this thesis, we have explored the dominant controls of legacy nitrogen accumulation in a predominantly agricultural 6000-km^2 mixed-landuse watershed. First, we synthesized a 216 year (1800 – 2016) nitrogen (N) mass balance trajectory at the subbasin scale accounting for inputs from population, agriculture, and atmospheric data, and output from crop production using a combination of census data, satellite imagery data, and existing model estimates. Using these data, we calculated the N surplus, defined as the difference between inputs to the soil surface from manure application, atmospheric deposition, fertilizer application, and biological N fixation, and outputs primarily from crop production. We then used the ELEMeNT-N model, with the estimates of the N mass balance components as the model inputs, to quantify legacy accumulation in the groundwater and soil in the study basin and 13 of its subbasins.

Our results showed that from 1950, N surplus across the study site rose dramatically and plateaued in 1980. Agricultural inputs from fertilizer and biological nitrogen fixation were the dominant drivers of N surplus magnitude in all areas of the watershed. Model results revealed

that 40% of the N surplus to the watershed since 1940 is stored as legacy N, and that the proportion of N surplus that is stored as legacy vary across the watershed, ranging from 33% to 69%. Where legacy tends to accumulate also varies across the watershed, ranging from 49% - 72% stored in soil, and 28% - 51% stored in groundwater. Through correlation analysis, we found that soil N accumulation tends to occur where there is high agricultural N surplus, and groundwater N accumulation tends to occur where mean groundwater travel times are long. We also found that using the model calibrated mean groundwater travel times as an indication of lag times, we can identify the length of lag time in various regions in the watershed to help inform long-term management plans. Our modeling framework provides a way forward for the design of more targeted approaches to water quality management.

Acknowledgements

I would like to thank the Legacies of Agricultural Pollutants (LEAP) project for providing me with financial support throughout my entire degree. I am grateful for the opportunity to learn and contribute to the project with little worry over finances.

First and foremost, I would like to thank my supervisor, Nandita Basu, for giving me the privilege of working with her and being part of her incredible lab. I would also like to thank Kim Van Meter, who worked closely with me during my most naïve times. I can never appreciate enough the amount of patience and guidance these two admirable women have spared for me throughout my degree. I have an immense appreciation for research from seeing your never-ending curiosity and dedication, and I hope to return to research one day when my mind has matured a little more and emulate your genius.

I would like to thank Kirsten Grant for her work on editing this thesis and always being welcoming and readily responsive to all of my technical and administrative problems.

I am so grateful to be part of a lab full of high-quality people. You have turned those long days and late nights in the lab into happy memories. Thank you for all the meme sharing, Friday afternoon chats, stress-relieving gymming, communal caffeine stock, and unintentional amusing quotes.

I thank my favorite people for cherishing me, being the reason I can reflect my namesake, helping me become strong physically, mentally and spiritually, and making Waterloo a place for me to miss.

Finally, I would like to thank my mom and dad for allowing me to choose my own way, to learn from my own mistakes, and for having faith in me when things do not go smoothly. I hope I can continue to make your sacrifices worth it.

Table of Contents

List of Figures

List of Tables

Chapter 1 Introduction

1.1. Eutrophication and algal blooms

The eutrophication of rivers, lakes, and coastal regions around the world have have been attributed to excess nutrient loading from human activities including urbanization, industrial processes, and agricultural activities (Carpenter et al., 1998; Heisler et al., 2008). Nitrogen (N) and phosphorus (P) are two limiting nutrients in aquatic ecosystems that are released into the environment through wastewater treatment plant effluent discharges, atmospheric deposition of nitrogen in fossil fuel emissions, and nonpoint source pollution from fertilizer runoff and leaching into the groundwater (Boyer et al., 2002; Di and Cameron, 2002; Kleinman et al., 2011; Mekonnen and Hoekstra, 2018). Excess nutrient loading is often linked increased algal blooms, some of which can be toxic, and often leads to the formation of hypoxic 'dead zones' (Dodds, 2006). Instances of harmful algae blooms (HABs) and algae-induced hypoxia in both freshwater and coastal waters have been documented all over the world, including Lake Taihu in China (Paerl et al., 2011), the Gulf of Mexico in North America (Turner et al., 2008), lakes and coastal waters in Denmark (Kronvang et al., 2005), and Lake Erie of the Laurentian Great Lakes (Watson et al., 2016).

1.2. Water quality mitigation efforts appear to yield disappointing results

Within the last 50 years, efforts have been made to mitigate the growth of algal blooms by upgrading wastewater treatment plants, which have led to to significantly reduced point-source phosphorus, and implementing atmospheric emission reduction policies, which have led to reduced nitrogen deposition (Lloret and Valiela, 2016; Maccoux et al., 2016). The focus has now shifted to controlling nonpoint sources of nutrients by implementing agricultural best

management practices (BMPs), which have shown successful reduction of nutrient loss from the field (International Joint Commission, 1983; Kaika, 2003; Liu et al., 2017; Mitchell and Shrubsole, 1992; Zbieranowski and Aherne, 2011). Despite these advances, targets for watershed-scale nutrient reduction have not been met (Carpenter et al., 1998; Sharpley et al., 2009; Sprague and Gronberg, 2012; Worrall et al., 2009). Reducing nonpoint source nutrient loading at the watershed-scale appears to be disconnected from field-scale success, and has been proven a challenging goal (Liu et al., 2017). Notably, there have been extensive efforts in the Mississippi and the Chesapeake Bay to reduce N loading for more than 20 years by wide implementation of BMPs, but neither reached their target loads (Van Meter et al., 2018). In Europe, only 31% of designated Nitrate Vulnerable Zones had improved water quality, and the rest either saw no significant water quality or even experienced increased nitrate loadings after 12 to 15 years (Worrall et al., 2009). In the Maumee and Sandusky, two major tributaries of Lake Erie, there have been no significant long-term trends in reduced N concentrations despite decades of non-point source control measures being implemented (Choquette et al., 2019).

1.3. Lag times and legacy responsible for disappointing water quality results

These apparent failures in water quality improvement despite decades of efforts is increasingly attributed to watershed-scale lag times (Liu et al., 2017; Meals et al., 2010). Nutrient lag time is the time it takes for implementation of BMPs to translate into downstream water quality improvements, which can range between 5 to more than 50 years (Meals et al., 2010). Without consideration for lag times, expectations for water quality improvements are often given an unrealistically short timeline. Unmet expectations may lead to the false perception that BMPs are not effective and halt further funding and implementation (Meals et al., 2010). Lag times can

arise when N accumulated on the landscape are released into streams over sub-annual to decadal timeframes (Hamilton, 2012; Van Meter and Basu, 2017). Inorganic N can be stored in the unsaturated zone of the soil profile, and more importantly in groundwater, which can have residence times from days to decades depending on length of flow path and type of substrate (Hamilton, 2012). Van Meter and Basu (2015) conceptualized this store as the hydrologic legacy, which includes both N in groundwater and dissolved inorganic N in the unsaturated zone of the soil profile. Van Meter and Basu (2015) also conceptualized a biogeochemical lag time where N is accumulated in the root zone as an organic form, where it can mineralize over time and transfer to the hydrologic legacy. In contrast to the widely accepted hydrologic legacy, the biogeochemical legacy is still a topic under scrutiny, but an increasing number of studies are uncovering evidence for its significance in long-term watershed N dynamics (Sebilo et al., 2013; Van Meter et al., 2016). Thus, it is pertinent to quantify lag times and legacy stores to make informed plans and policies for mitigating the effects of eutrophication.

1.4. *Recent advances in lag time modelling*

Since lag times can often span timeframes greater than existing measured data, modelling tools can be used to make estimates (Bouraoui and Grizzetti, 2014). Traditional modelling frameworks however, do not consider lag times. Existing models for assessing changes in water quality in response to changes in N inputs can be categorized as empirical, conceptual, and process-based (Bouraoui and Grizzetti, 2014). Empirical models, such as the Net Anthropogenic Nitrogen Input (NANI) based models, are the simplest of the models, and they draw statistical relationships between N inputs and outputs in stream N loading, while considering all physical processes as a black box. Traditional process-based models, such as the Soil Water Assessment

tool (SWAT), are the most complex, and are designed to predict the final reduction in stream concentration as a result of BMP implementation using physically based processes, but does not model the time it takes to reach those states (Ilampooranan et al., 2019). Finally, conceptual models, notably Geospatial Regression for European Nutrient Losses (GREEN) and MOdelling Nutrient Emissions in River Systems (MONERIS) are those of intermediate complexity, and may consider multiple nutrient transfer pathways and simplified representations of key nutrient processes, but are limited by the traditional framework of the lack of consideration for lag times (Bouraoui and Grizzetti, 2014; Van Meter et al., 2017). Without such estimations of lag times, policy makers are missing an important piece of information to make feasible long term plans that will effectively achieve final water quality targets.

Recently, there have been attempts to adapt empirical and conceptual models to account for lag time, such as NANI (Hong et al., 2017) and MONERIS (Behrendt et al., 2000). However, they are unable to account for the different physical behaviours of both the hydrologic and biogeochemical legacy pools, and therefore model lag times explicitly (Behrendt et al., 2000; Hong et al., 2017). As a result, it is inadequate for predicting outputs under significantly different input regimes, and identify sources of uncertainty associated with modelled results (Chen et al., 2018; Van Meter et al., 2017). The process-based model, SWAT, has also recently been adapted for modelling nutrient lag times, but its complexity and high parameterization may be restrictive for wide adoption in watersheds with less data (Chen et al., 2018; Ilampooranan et al., 2019).

In 2015, Van Meter and Basu developed a framework for process-based modelling of Legacy N to quantify lag times. Their model ELEMeNT (Exploration of Long-Term Nutrient Trajectories) operated under this framework, and has since been used to estimate lag times and size of legacy stores for a number of watersheds (Van Meter et al., 2018, 2017). ELEMeNT operates by pairing

a long-term input trajectory of N with a source zone dynamic function coupled with a groundwater travel time distribution approach, to simulate N retention and transport in surface and subsurface pathways, to determine stream N loading trajectories at the watershed outlet. Using such approach, Van Meter et al., (2017) modelled N dynamics of the Mississippi watershed from 1800 to 2014, and found that 55% of the the current annual stream N loading was more than 10 years old, and in Van Meter et al., (2018), it would take between 7 to 25 years under various N reduction scenarios to achieve the 20% target in reduction of stream loading to the Gulf of Mexico.

1.5. Eutrophication in the Lake Erie and need for dual nutrient controls

Of the five Laurentian Great Lakes, Lake Erie experiences the most visible symptoms of eutrophication due to its high nutrient input from its basin and shallow bathymetry leading to warm waters (Ho et al., 2017). A record setting algal bloom event was recorded in 2015, with an area of over 2000 square kilometers (Ho et al., 2017). The event illuminated the increasing severity of eutrophication in the lake. The lake is important to the local economy. One study estimating the blooms cost the local economy $270 million per year, when considering the costs of finding substitute sources of drinking water, and losses in the tourism and recreation sector (Smith et al., 2019).

Research in the 1960s and 70s found that excess nutrient loading, particularly for phosphorus (P) was the cause of eutrophication and algal blooms (Beeton and Edmondson, 1972; Davis, 1964). Efforts to reverse cultural eutrophication in Lake Erie sparked the development of the 1972 Great Lakes Water Quality Agreement (GLWQA) (International Joint Commission, 1970, 1965). The

GLWQA outlined the responsibilities of the U.S. and Canada to reduce nutrient input, particularly P, from watersheds within their respective borders.

Activities stemming from the agreement focused on the aggressive elimination of point source P, primarily by upgrading wastewater treatment plants and eliminating P from detergents (Dolan, 1993). As a result, the lake appeared to have recovered from eutrophication in the 1980s (Allinger and Reavie, 2013). However, massive algal blooms seemed to recur within a decade, despite continued efforts in restricting P inputs from both point and non-point sources (International Joint Commission, 1983; Richards et al., 2002).

More recent findings on the ecology of Lake Erie suggest that only controlling phosphorus is no longer adequate, although this is a hotly debated topic (Paerl et al., 2016; Schindler et al., 2016; Watson et al., 2016). Proponents of P-only control argue that it is a cost-effective, feasible strategy to mitigate algal blooms due to eutrophication (Schindler et al., 2016). They cite long-term whole-lake case-studies showing the success of P-only nutrient management (Dove and Chapra, 2015; Fastner et al., 2016; Schindler, 1974). The re-eutrophication of Lake Erie was also thought to be due to poor control of P from non-point sources and internal lake cycling, and not due to the lack of N control (Schindler et al., 2016). Contrary to the P-only control paradigm, a growing body of literature suggests that in some freshwater ecosystems, N must be reduced concurrently with P (Conley et al., 2009; Lewis and Wurtsbaugh, 2008; Paerl et al., 2016). Dual-nutrient control of N and P considers specific characteristics of a freshwater aquatic ecosystem beyond assumed P limitation. They showed that N and P fertilization was more effective in stimulating algal growth in a spectrum of scales, from microcosm to whole-lake experiments, than fertilization of either nutrient alone (Elser et al., 2007; Fee, 1979; Paerl et al., 2016). Furthermore, high N-P ratios have been found to be a driver of HAB formation in the central

basin of Lake Erie (Chaffin et al., 2019; Gobler et al., 2016). Finally, controlling N in addition to P may have holistic effects on downstream waters which are vulnerable to increased N inputs (Paerl et al., 2016). This includes N-limited estuaries and coastal ecosystems, or ecosystems that have the right conditions for nitrate-induced P mobilization (Paerl et al., 2016; Smolders et al., 2010). It is becoming clear that controlling the nitrogen (N) loading may be essential for the health of the lake as well.

There are currently no official N reduction targets set, nor are there limits set for stream nitrate concentration by governing authorities in the province of Ontario, where the Canadian side of the Lake Erie basin lies (Ministry of Environment, and Energy (MOE), 1994). However, there have been recommendations to set targets for stream nitrate concentrations for ecosystem health (Grand River Conservation Authority, 2013). In streams fed by groundwater, high stream nitrate concentrations may also indicate higher concentrations in groundwater (Tesoriero et al., 2009). Groundwater is a source of drinking water, which has nitrate limits of 10 mg/l. Thus, limiting nitrogen loss into groundwater and surface water as it not only has benefits for downstream ecosystems, but also in-situ benefits for the watershed ecosystem and its resources.

1.6. Thesis Objectives

The understanding of legacy nutrients in intensive agricultural watersheds is still in its early stages. In this thesis, we use the ELEMeNT model to better understand the drivers of N legacy accumulation and depletion along the river continuum by applying the model to multiple sub-basins within a 6800 km^2 highly agricultural watershed draining into Lake Erie. The objectives of the thesis are to (1) synthesize a long-term trajectory of N mass balance, (2) quantify the magnitude of legacy N stores, and (3) find what physical landscape characteristics drive N

accumulation and the associated lag times. The findings of the study will be used to provide recommendations for management strategies that minimize lag times and maximize water quality benefits through targeted implementation.

Chapter 2 ELEMeNT Modelling Framework

2.1. *Legacy nutrients and land-use change dynamics*

The ELEMeNT-N (Exploration of Long Term Nutrient Trajectories for Nitrogen) model has been used to model water quality across the land-aquatic continuum in various coastal watersheds in the U.S. (Van Meter et al., 2018, 2017, 2015). The model utilizes a coupled framework that links source-zone dynamics, describing the accumulation and depletion of soil organic nitrogen (SON) within the root zone, with a travel time model that describes transport and transformations along hydrologic pathways to the stream outlet (**Figure 1**).

The model operates on the principle that N dynamics in the soil is a function of both current and past land use and land management trajectories (Van Meter et al., 2017). ELEMeNT considers the effect of current-year N inputs onto the landscape, as well as the role of legacy N stores on stream N fluxes, and this critical factor distinguishes it from other watershed models. To do this, each landscape unit in the ELEMeNT model is allowed to retain a memory of past land use and land management. For example, two landscape units may both be non-agricultural land at the current time, but one may have converted from cropland in 1950 and the other in 1970. These two units represent two different land use trajectories, with differing N legacies, and therefore differing contributions to the current year N fluxes through the watershed. The ELEMeNT framework is unlike common nutrient modelling approaches that do not explicitly consider long term changes in land use and management.

2.2. Travel time-based approach to modelling outlet N loading

To quantify the nitrate-N loading trajectories at the watershed outlet following land use change, ELEMENT-N conceptualizes the landscape as a bundle of stream-tubes, each with a unique travel time to the watershed outlet, such that the landscape as a whole can be characterized by the travel time distribution f(τ) (McGuire and McDonnell, 2006; Van Meter et al., 2017). The N load [M/L2/T] at the watershed outlet is thus calculated by convoluting the N flux from each of the stream tubes as:

$$M_{out}(t) = \int_0^{\infty} J_s(t-\tau) f(\tau) e^{-\gamma\tau} d\tau + (1-k_h) W(t) \qquad (1)$$

where $M_{out}(t)$ is the N loading at the outlet in year t [M/L^2/T]; $J_s(t - \tau)$ is the source function, which describes the flux of nitrate-N from the source zone to the groundwater (Section 2.3)[M/L^2/T]; $f(\tau)$ describes the chosen travel time distribution, such as the exponential or lognormal, where τ is the travel time [T]; γ is the first-order rate constant that describes N removal via denitrification along hydrologic pathways [T^{-1}]; $W(t)$ is domestic waste [M/L^2/T]; and k_h is the N removal rate constant from domestic waste via denitrification [T^{-1}] (Section 2.5). It should be noted that wastewater N inputs, described by the second term in Equation (1), are considered to directly enter surface water, with negligible travel times to the catchment outlet. We assume that N transport through erosion of particulate N is negligible, due to the high solubility of N compounds.

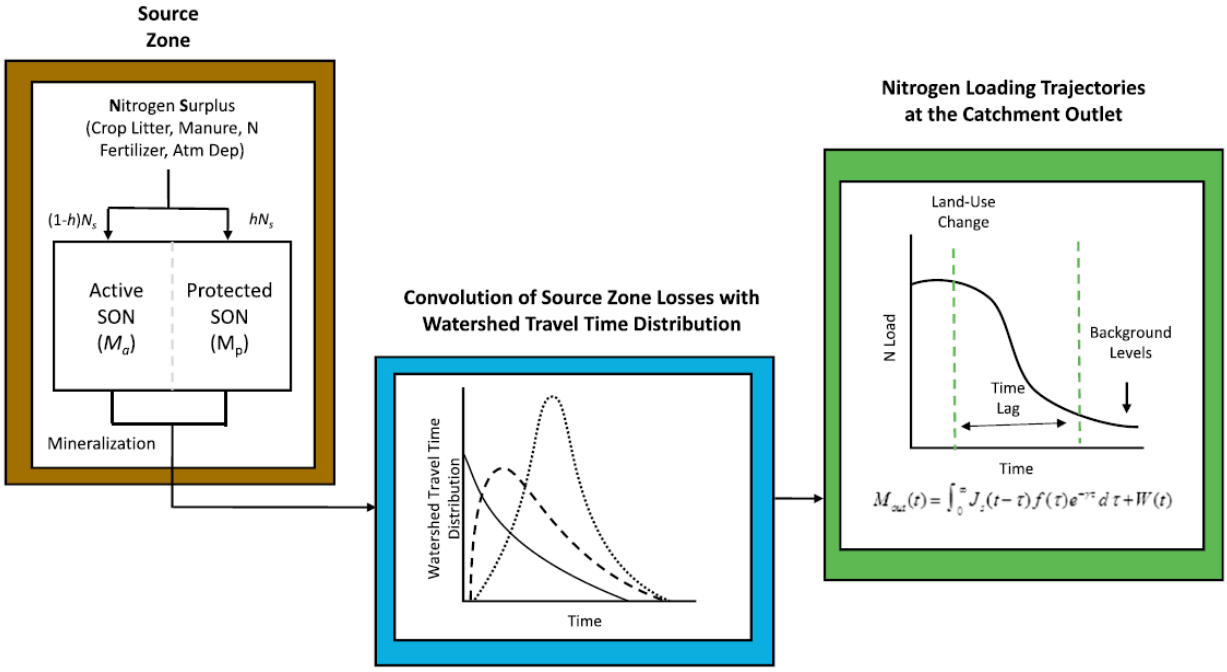

Figure 1. Conceptual ELEMeNT-N framework for travel-time based approach to modelling The source zone (left box) is where N flows through soil organic matter which can accumulate and deplete as biogeochemical legacy. Here, *Ns* represents the annual N surplus described in Section 3.3,and *h* is the protection coefficient which allocates N surplus into the more mobile, active SON, and the more stable, protected SON pools. Mass depletion from the source zone occurs through leaching of mineralized N and enters the groundwater pool (middle box). The N is convoluted with the groundwater travel time distribution to describe the annual N loading at catchment outlet (right box). (Diagram source: Van Meter et al., 2017)

2.3. Source zone dynamics

The source zone represents the root zone where N cycles through SON where it can be mineralized into inorganic N. Leaching processes from the source zone transports inorganic N into the groundwater through the source function $J_s(t - \tau)$. In this section, we describe how the source function is estimated from N inputs to the landscape over time, using watershed land use trajectories and associated biogeochemical processes.

2.3.1. Watershed Land Use Trajectories

In ELEMeNT, the watershed is broken up into land use units indexed here as *s*. Each unit is assigned a distinct land use trajectory representing transitions in land use over time, *t*. ELEMeNT considers land use to be categorized as cropland, pastureland, and non-agricultural land. The land use trajectories for each unit is stored in a 2-D land use array, *LU(s, t)*, developed using the following expression,

$$LU(s,t) = \begin{cases} 1 & s \le A_{crop}(t) & \text{cropland} \\ 2 & A_{crop(t)} < s \le \left[A_{crop}(t) + A_{past}(t)\right] & \text{pastureland} \\ 0 & s > \left[A_{crop}(t) + A_{past}(t)\right] & \text{non-agricultural} \end{cases} \quad (2)$$

Where *LU(s, t)* is the land use array; *s* is the index of each unit; *t* is the modelled year; and A_{crop} and A_{past} are the watershed-scale percent areas of cropland and pastureland, respectively, based on land use trajectories. This expression assigns values to the land use array, where 1 represents cropland, 2 represents pastureland, and 0 represents non-agricultural land. The watershed-scale land use trajectories are generated based on databases created from satellite imagery and modelled historical estimates of crop and pastureland, described in detail in Section 3.5.

2.3.2. Estimation of the Source Function

Each of the *s* land use units have a corresponding source zone function, $J_{ls}(s, t)$, to describe the mass flux of nitrate-N leaching from the unsaturated zone to the groundwater at any time *t*. The watershed-scale source function *Js(t)* used in Equation (1) can then be estimated as the sum of the fluxes across all land use units as:

$$J_s(t) = \sum_{s=1}^{RES} J_{ls}(s, t) \qquad (3)$$

Where *RES* is the user defined resolution of land use units with recommended values ranging from 100 to 1000.

The source function for each land use unit *s*, $J_{ls}(s, t)$, can be estimated as a function of the legacy mass residing in the source zone **(Figure 2)**. The mass residing in the source zone is the sum of the mass in the soil organic matter, $M_{SON}(s, t)$, and the mass in the mineral pool, $M_S(s, t)$. The soil organic matter pool is made up of the sum of the active and protected SON pools, $M_a(s, t)$ and $M_p(s, t)$, respectively.

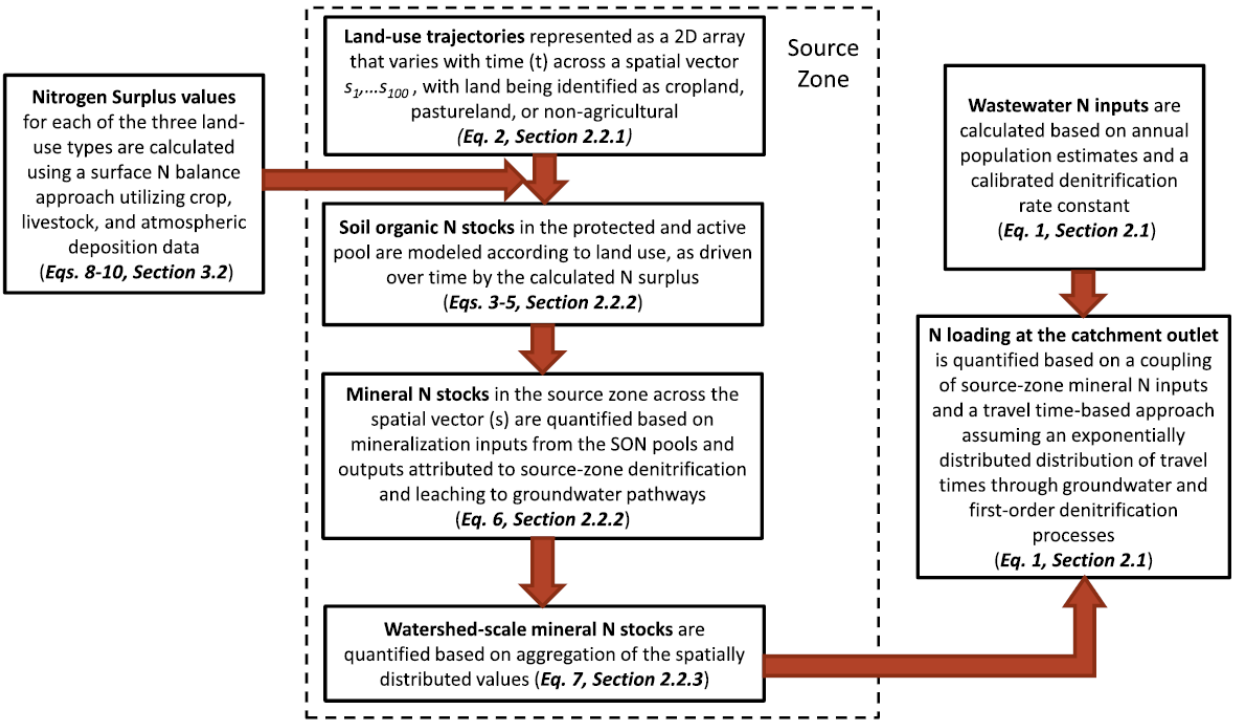

Figure 2. The ELEMeNT Modelling Framework. (Source: Van Meter et al., 2017)

Within this framework, we consider that all of the annual N surplus (Ns (i, t), kg/ha/t, i = 0, 1, 2 for the three different land use studied) cycles through either the active or the protected SON pools, where it can be mineralized into nitrate-N. This pathway is consistent with isotope studies which indicate that the majority of nitrate-N leachate undergoes biogeochemical transformation in soil organic matter (Haag and Kaupenjohann, 2001; Spoelstra et al., 2001; Van Meter et al., 2017). The active pool represents the more mobile forms of SON with faster reaction kinetics, while the protected pool represents the recalcitrant forms of N with slower kinetics. For each land use unit, the model allocates N surplus to the two SON pools using a protection coefficient, '*h*', which is differentiated for cultivated land (h_c for LU = 1,2) and non-cultivated land (h_{nc} for LU = 0). The protection coefficients represent physical protection mechanisms such as soil aggregation, which varies between land use types due to differences in land management and

tillage practices (Janssen, 1984; Six et al., 2002; Van Meter et al., 2017). Mineralization of SON is conceptualized as a first-order rate process via microbial activity. To address the differing metabolics of each SON pool, we define two mineralization coefficients: k_a for the active SON pool and k_p for the protected pool. The N dynamics for the SON pools across the distribution of land use trajectories can then be described by the following differential equations:

$$\frac{dM_p(s,t)}{dt} = \begin{cases} hN_s(LU(s,t),t) - k_p M_p(s,t), LU(s,t) = 0,2 \; and \; LU(s,t-1) = 1 \\ hN_s(LU(s,t),t) - \left(M_{p(s,t)} - 0.7M_{p_{prist}}\right), LU(s,t) = 1 \; and \; LU(s,t-1) = 0,2 \end{cases} \quad (4)$$

$$\frac{dM_a(s,t)}{dt} = \begin{cases} (1-h)N_s(s,t) - k_a M_a(s,t), LU(s,t) = 0,2 \; or \; LU(s,t) \; and \; LU(s,t-1) = 1 \\ (1-h)N_s(s,t) + \left(M_p(s,t) - 0.7M_{p_{prist}}\right), LU(s,t) = 1 \; and \; LU(s,t-1) = 0,2 \end{cases} \quad (5)$$

Where *Ma(s, t)* and *Mp(s, t)* are the active and protected SON pools, respectively [M/L^2]; Mp_{prist} is the protected SON stocks under pristine land use conditions [M/L^2]; *Ns(LU(s, t),t)* is the N surplus array, representing the land use specific *Ns* value for year *t*, as calculated in Section 3.3. [M/L^2]; *LU(s, t)* is the land use array, developed in Section 2.3.1; k_a and k_p are the mineralization rate constants for active and protected SON, respectively [T $^{-1}$]; and h is the humification rate constant, also known as the protection coefficient [T $^{-1}$]. The values of k_a, k_p, *h*, and Mp_{prist} are determined through calibration, detailed in Section 3.8.

Our framework addresses how changes between cultivated and non-cultivated land affect SON stocks. We consider the protected SON pool to remain intact via physical mechanisms such as soil aggregation. As such, the ploughing of non-cultivated land through land use conversion disturbs the physical protection mechanisms and mobilizes the protected SON stocks (Six et al., 2002). Thus, land use transitions from pastureland (LU = 2) or non-agricultural land (LU = 0) into cropland (LU = 1) releases SON from the protected pool and into the active pool in a step function. We assume the magnitude of the step transfer to be 70% of the SON content under

pristine conditions (Mp_{prist}), based on empirical evidence of SON depletion of this magnitude on landscapes after initial cultivation (Beniston et al., 2014; Davidson and Ackerman, 1993; Van Meter et al., 2017; Whitmore et al., 1992). The mass transfer into the active SON pool subjects the N to faster mineralization via k_a. Thus, under the modelling framework, active and protected SON stocks are partitioned both as a function of land use type and the cultivation of land, as governed by Equations (4) and (5).

SON that is mineralized in the source zone exists as the mineral N pool, primarily in the form of nitrate-N. The loss of mineral N occurs through soil denitrification and groundwater leaching. The source zone mineral N dynamics and the source zone mass flux into the groundwater for every land use unit, *s*, are described by the following equations

$$\frac{dMs(s,t)}{dt} = k_a M_a(s,t) + k_p M_p(s,t) - \lambda M_s(s,t) - J_{ls}(s,t) \quad (6)$$

$$J_{ls}(s,t) = \begin{cases} M_s(s,t)\dfrac{Q(t)}{V_w}, & Q(t) < V_w \\ M_s(s,t), & Q(t) > V_w \end{cases} \quad (7)$$

Where M_s is the source zone mineral N pool [M/L^2]; λ is the denitrification rate constant in the source zone [T^{-1}], $J_{ls}(s, t)$ is the stream-tube scale source function describing the flux of mineral N to groundwater [M/L^2], $Q(t)$ is the annual stream discharge [L/T], and V_w is the volume of water in soil column [L].

The first and second terms on the right-hand side of Equation (6) represent the mass input to the source zone mineral N pool (M_s) from SON mineralization. The third term describes the N loss from M_s due to denitrification, λ as the first-order rate coefficient. The final term, $J_{ls}(s, t)$, describes the stream-tube scale loss of N to groundwater, detailed in Equation (7). Mineral N in the source zone is assumed to leach proportionally to the ratio of stream discharge $Q(t)$ to

saturated soil water volume V_w. Note that under this scheme, if $Q(t)$ exceeds V_w, the source zone mineral N pool is considered to be completely flushed into the groundwater. The volume of water in saturated soil V_w is calculated using an average soil porosity (n), field capacity (θ), and soil column volume depth of 1m. Soil properties were determined using data from Landscapes of Canada and is detailed in Section 3.7.

2.4. Travel time distribution

Under the ELEMeNT framework, mineral N that enters the groundwater from the source zone via leaching is considered to travel with groundwater flow as nitrate-N. The groundwater flow is modelled by stream-tubes, each with unique travel times sampled from a chosen distribution. In the current version of the model we assumed an exponential travel time distribution, though other forms of a travel time distribution, such as gamma and lognormal distribution, can also be considered.

$$f(\tau) = \frac{1}{\mu} e^{-\frac{\tau}{\mu}} \qquad (8)$$

Where $f(\tau)$ is the probability distribution function, τ is the travel time [T^{-1}], and μ is the characteristic mean of the distribution, or mean travel time [T^{-1}]. The distribution parameter, μ, is a calibrated parameter.

2.5. Domestic wastewater input

The last component of the nitrate-N mass flux trajectory in Equation (1) is domestic waste. The production of domestic waste is calculated using human population and N consumption rates as a proxy. The estimation of total waste production is described in detail in section 3.3.2. We assume

that all domestic waste routes through wastewater treatment plants (WWTPs) and enters streams as wastewater effluent. Thus, we consider denitrification in the WWTP and in-stream processes with an effective denitrification parameter, k_h. The value of k_h is determined through calibration. Since effluent from WWTPs is discharged directly into streams, ELEMeNT routes it directly to the outlet, bypassing the SON processes and groundwater travel.

Chapter 3 Methods and Data Sources

3.1. Study Area

The Grand River Watershed (GRW), located in southwestern Ontario, is the largest Canadian watershed draining into Lake Erie, with an area of approximately 6800 km^2 (Grand River Conservation Authority, 2008). It is the 4th largest tributary contributing nutrients into Lake Erie, making it important to consider when reducing nutrient loads to Lake Erie (Maccoux et al., 2016). The land use in the watershed has gone through dramatic changes over the last 200 years, and today, about 60% of the watershed is used for agriculture **(Figure 5)**. The rest of the area is occupied by rapidly growing urban areas focusing around 3 main centres – Kitchener-Waterloo Region, City of Guelph, and City of Brantford. These 3 urban centres are located in the central, east, and southern part of the basin, shown in red in **Figure 3b**, where 90% of the watershed's population reside. The watershed also constitutes 10 administrative regions, called counties. A First Nations Reserve is also situated in the watershed. It is home to the indigenous people of the Six Nations of the Grand River, who have a separate legislative and data reporting structure than the rest of the counties. To support its population, the watershed contains 30 wastewater treatment plants serving 85% of the nearly 1 million people (The Grand River Conservation Authority, 2008). River flows within the GRW are managed by 7 major dams and reservoirs along the Grand River and its tributaries (Grand River Conservation Authority, 2014).

Land use and soil characteristics vary across the drainage basin, as shown in **Figure 3**. Its soils are formed through repeated glacial advances and retreats, leaving uneven deposits of tills, gravel, sand, and clay, lending to varying hydraulic characteristics. In the north and northwest, there are the Till Plains with extremely low hydraulic conductivity, high conductivity till

moraines and sands in the central basin, and a low conductivity clay plain in the south **(0c)**. The dense installation of tile drains in the poorly drained regions allow for agriculture across the watershed (**0 (a)**).

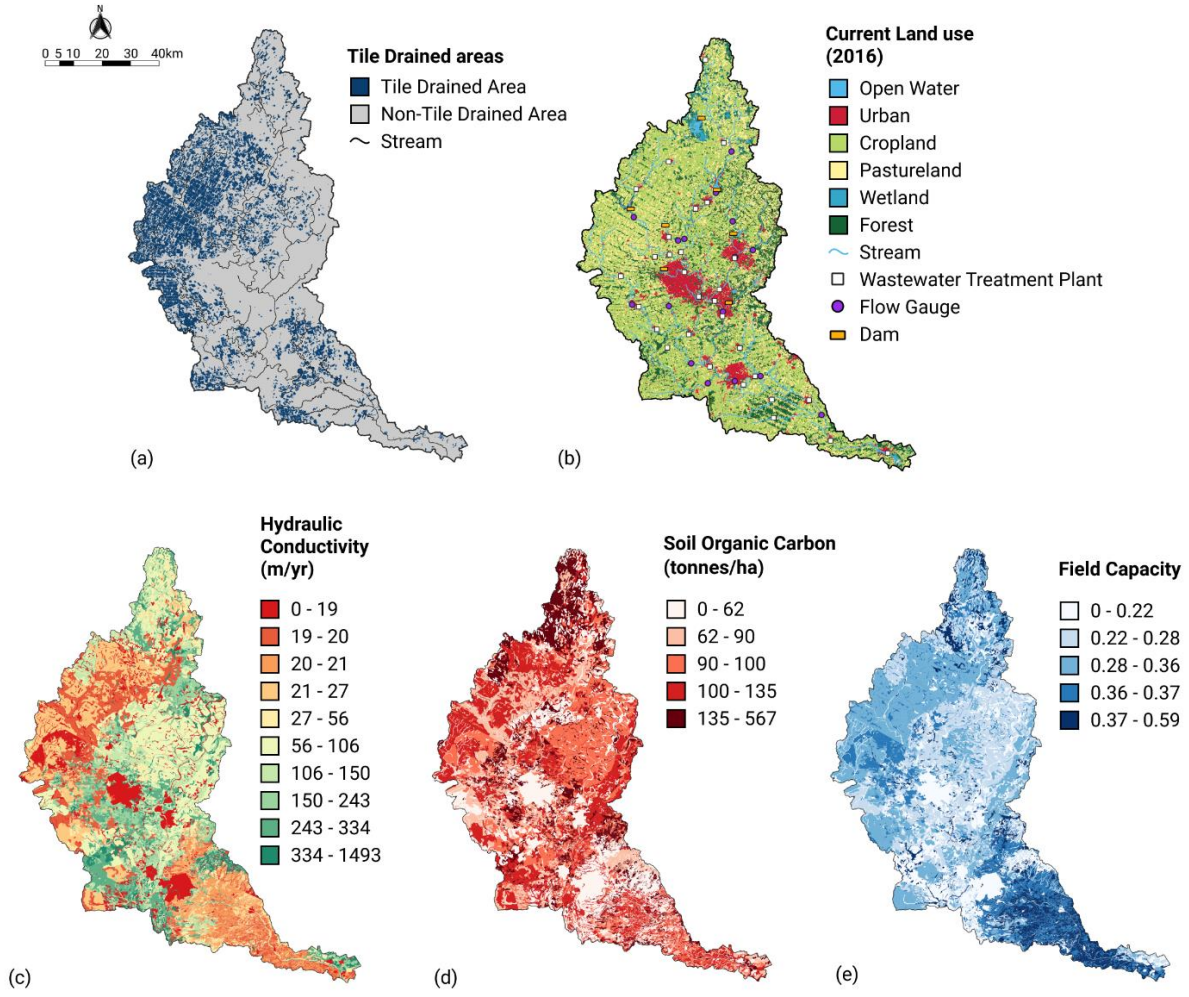

Figure 3. Spatial physical characteristics of the Grand River Watershed. Soil characteristics shown in (c) to (e) show depth-weighted averages of the first 100cm

.

3.2. Model Domain

Since the goal of our study was to quantify spatial patterns in nitrogen legacy stores across the landscape, we first identified streamflow and water quality stations that had adequate long-term data. Daily discharge data was obtained from the Canadian Hydrometric Database (National Hydrological Service, 2016), while water quality data was obtained from the Provincial Water Quality Monitoring Network (PWQMN) database (Ministry of Environment and Climate Change, 2016). PWQMN monitoring stations were selected based on the following criteria: (1) availability of at least 20 years of data, and (2) proximity to a MOE flow monitoring station. Flow and water quality stations were paired if there was less than 10% difference in drainage areas of the two stations. The final accepted 14 basins had 35 to 51 years of paired discharge and stream concentration data, and a summary of paired flow and water quality stations is listed in **Table 1**. Of these 14 basins, we developed our model for 7 headwater subbasins, 6 downstream basins, and the entire GRW (**Table 1** and **Figure 4**). As shown in **Figure 4b**, we modeled 6 subbasins along the mainstem of the Grand River to quantify how processes and parameters change along the network. Unlike previous uses of ELEMeNT, which was applied to whole single watersheds, the application of ELEMeNT in this thesis is to model nested subbasins of a watershed (Van Meter et al., 2018, 2017; Van Meter and Basu, 2015). As such, we must consider calculating input data on a finer scale, and nested basin effects.

Table 1. Subbasin Info

Subbasin Name	Flow Station ID	Water Quality Station ID	Basin Size (km^2)
Canagagigue Creek	2GA023	16018401602	113
Conestogo River	2GA028	16018407702	566
Whitemans Creek	2GB008	16018410602	395
Nith, New Hamburg	2GA018	16018403202	542
Nith, Canning	2GA010	16018400902	1105
Eramosa River	2GA029	16018410202	228
Speed, Armstrong	2GA040	16018409902	177
Speed, Guelph	2GA015	16018403402	572
Grand, Marsville	2GA014	16018406702	656
Grand, Shand Dam	2GA016	16018403702	780
Grand, West Montrose	2GA034	16018410302	1148
Grand, Galt	2GA003	16018401002	3552
Grand, Brantford	2GB001	16018402402	5200
Grand, York	2GAC06	16018409202	6006

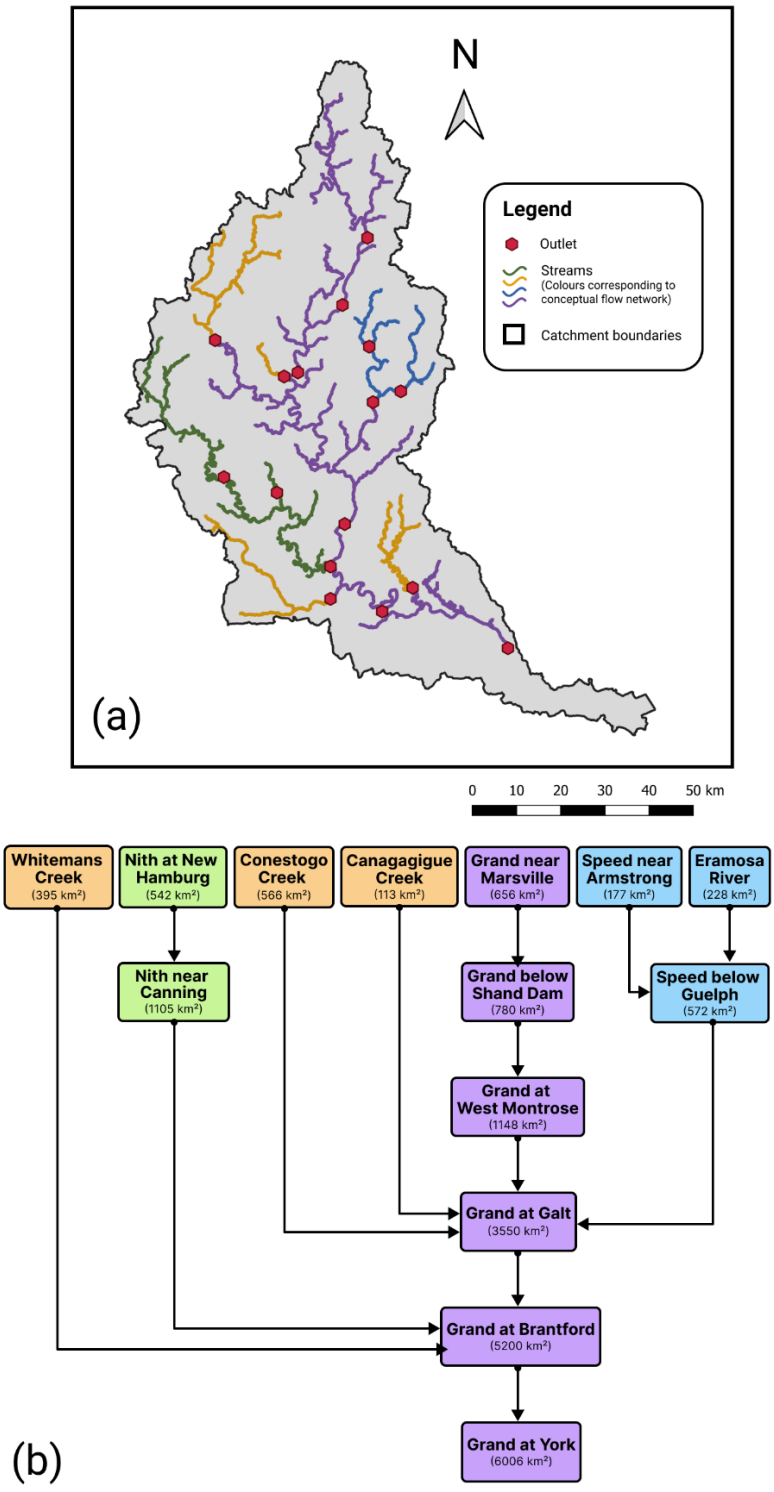

Figure 4. The Grand River Watershed Stream Network showing (a) mapped gauging station locations and (b) conceptual subbasin flow network. Colors of streams correspond with the colors of subbasin names in the flow chart.

3.3. Nitrogen Mass Balance

ELEMeNT requires a multi-decadal trajectory of the historical inputs and outputs of N, and land use for each subbasin. This section outlines how the data for each of these components were collected and synthesized to run the model. The data sources and time spans they cover are summarized in **Table 6**. Annual N surplus values were calculated using a surface N balance approach (Parris, 1998) that estimates N surplus as the difference between N inputs (livestock manure, mineral fertilizer, biological nitrogen fixation, and atmospheric N deposition), and N outputs (crop production and livestock pasture consumption) at the soil surface. The surplus trajectories are calculated separately for cropland, pastureland and non-agricultural land using the following equations:

$$N_s(crop,t) = MAN_{crop} + FERT_{crop} + BNF_{crop} + DEP - CROP \quad (9)$$

$$N_s(past,t) = MAN_{past} + BNF_{past} + FERT_{past} + DEP - GRASS \quad (10)$$

$$N_s(other,t) = BNF_{nat} + DEP \quad (11)$$

Where, N_s is the N Surplus applied to cropland, pastureland, or non-agricultural land at the soil surface; MAN_{crop} is the manure applied to cropland and MAN_{past} is the manure directly deposited onto pastureland during grazing; *FERT* refers to the applied mineral fertilizer; BNF is the biological nitrogen fixation by crops and natural vegetation; *DEP* is atmospheric N deposition, *CROP* is the uptake by harvested crops; and *GRASS* is the pasture consumption by grazing livestock, all expressed as kg N/ha land use/year.

3.3.1. Livestock Manure Inputs

Manure applied to the soil surface was calculated for crop and pasture land based on the methodology by Ruddy et al. (2006), who calculated manure production using county-level livestock population data and estimated N content of manure by livestock type. In this analysis, we collected data on 11 types of livestock, listed in **Table 2**. To estimate manure application to crop or pastureland, the population of each livestock type was collected from the Canadian Census of Agriculture, which had data every 10 years from 1901 to 1951, and every 5 years thereafter, at the county scale (Statistics Canada, 2016a). We also further divided the livestock into either unconfined or confined fractions based on Kellogg et al. (2000) and Smil (1999). Manure from unconfined livestock was considered to be directly applied onto pastureland. We assume that unconfined livestock graze on pastureland grasses during one-third of the year. The manure produced in confinement was assumed to be proportioned to cropland based on the fraction of cropland area in the subbasin. The remaining manure after cropland application is applied to pasture, provided it does not exceed the maximum recommended land application of 200 kg N/ha/year (Van Meter et al., 2017). Loss due to volatilization into ammonia was also accounted for, and assumed to be 36% of the total mass of the manure (Smil, 1999).

The manure N generated by each livestock species is calculated using the following equation,

$$MAN_a = POP_a \times N_{excr,a} \quad (12)$$

Where *POP* is the livestock population [heads]; and N_{excr} is the species specific N excretion rate (kg N/head/year).

The livestock population of each species is based on census data of county scale livestock population. The N excretion rate for each species is summarized in the table below.

Table 2. N Content in manure by livestock type

Livestock Type (heads)	N excretion rate (kg N / head / year)	Source
Beef Cows	78.80	Hofmann et al., 2006
Dairy Cows	122.00	Hofmann et al., 2006
Heifers	52.20	Hofmann et al., 2006
Steers	78.80	Hofmann et al., 2006
Bulls	90.10	Hofmann et al., 2006
Calves	25.30	Hofmann et al., 2006
Swine	7.20	Hofmann et al., 2006
Sheep and Lambs	7.00	Hofmann et al., 2006
Chickens	0.42	Hofmann et al., 2006
Turkeys	2.27	Hofmann et al., 2006
Horses and Ponies	49.30	Hofmann et al., 2006

3.3.2. N in Mineral Fertilizer

The fertilizer component of the mass balance refers to the mineral N fertilizer applied to cropland or pastureland. To estimate the total amount of fertilizer applied to each of the subbasins, we used fertilizer sales data available at the provincial scale to calculate an average provincial application rate (Statistics Canada, 2016b). We assume that all fertilizer sold was applied onto the landscape within the year. The average application rate was multiplied by the county-level crop area collected from the Canadian Census of Agriculture to get the quantity of fertilizer applied in each county. To account for crop land that is unevenly distributed across a county, we used a crop scaling parameter, detailed in Section 3.3.6. This county-scale fertilizer data was then aggregated to subbasins and distributed to cropland and pastureland based on land use area fractions. Fertilizer sales data was available annually from 1951 to 2016 (Statistics Canada, 2016b). Mineral N fertilizer was applied on crop land only in minute amounts until

1945, when new technology allowed mineral N to be synthesized at an industrial scale. Thus our estimated N fertilizer trajectory starts in the year 1945, at the end of WWII and beginning of the popularization of the Haber-Bosch Process. Fertilizer application between 1945 and the first fertilizer sales data point was linearly interpolated. Despite having annual data starting from 1966, we use only the fertilizer data in years where there is crop area data from the census. Fertilizer application between census years was linearly interpolated. We do this to avoid misrepresentation of the N surplus due to annual variations in fertilizer data where annual crop production data is unavailable. The application rate of fertilizer to pastureland was calculated as a fraction of the total subbasin fertilizer. The remaining fertilizer is considered to be applied to cropland.

3.3.3. Biological N Fixation

Biological N fixation (BNF) refers to the N converted from non-reactive atmospheric N into reactive forms of N in the soil (Galloway et al., 1995). In our analysis, we account for the BNF by cultivated crops and plants found on non-cultivated land. Major N-fixing crops in the GRW are beans, alfalfa, hay, and soybeans. Crop production is calculated in section 3.3.5 using data from the Canadian Census of Agricutlure (Statistics Canada, 2016a). The amount of N fixed by these crops were calculated using a yield-based approach (Haejin Han and J. David Allan, 2008), described in Equation 13.

$$BNF = P_{crop} \times N_{crop} \quad (13)$$

Where BNF_{crop} is mass of N fixed by the crop [M]; P_{crop} is the mass of crop produced, calculated in section 3.3.5 [M] as calculated in Section 3.3.5; and N_{crop} is the mass fraction of N fixation [M/M], summarized in **Table 3**.

Table 3. N Fixation rates

Crop	Fixation rate (kg N / kg crop / year)	Reference
Alfalfa	0.031	(Hong and Swaney, 2013)
Beans	0.095	(Zhang, 2016)
Hay, other	0.003	(Hong and Swaney, 2013)
Soybeans	0.066	(Hong and Swaney, 2013)

3.3.4. Atmospheric N Deposition

Atmospheric N exists in oxidized (nitrates) and reduced (ammonia) forms, and can be deposited to land through wet and dry processes. We estimated the historical N deposition by using data from the National Atmospheric Chemistry (NAtChem) database from 1980 to 1995 (NAtChem, 1995) with Hember's (2018) modelled N deposition (NACID-NDEP1) database that spans 1860 to 2013. Since the NACID-NDEP1 database uses NAtChem data starting in 1990 and we had NAtChem data from 1980, we used NAtChem to calculate the deposition from 1980 to 1989 to enhance the detail of the NACID data during that timeframe. NAtChem station data was used to estimate wet deposition rate by area using an inverse distance function, aggregated at the county scale. We then used data spanning 1990 to 1995 from NACID-NDEP1 and NAtChem, aggregated at the county scale, to calculate an average dry-to-wet ratio. This ratio was used to estimate the total N deposition from both wet and dry processes for the period from 1980 to 1989. We then use the 1980 N deposition rate to scale the NACID-NDEP1 database so that it is

consistent with local observations. Finally, we use the 2013 estimation for the years 2014 to 2016.

3.3.5. Crop and Pasture N Uptake

Nitrogen is removed from cropland through harvested crops, and from pastureland through grazing livestock. Crop uptake is calculated using a yield based approach for all major field crops in the GRW summarized in **Table 4**, via the following equation,

$$UPTAKE_{crop} = P_{crop} \times DM_{crop} \times NC_{crop} \quad (14)$$

Where $UPTAKE_{crop}$ is the mass of N uptake for a particular crop type [M], P_{crop} is the harvested crop mass [M], DM_{crop} is the crop dry matter mass fraction [M/M], and NC_{crop} is the nitrogen content fraction [M/M].

The harvested mass, P_{crop}, is calculated using data on crop specific cultivated areas from the Canadian Census of Agriculture (Statistics Canada, 2016a), which had data every 10 years from 1901 to 1951, and every 5 years thereafter, and data on crop yield (Statistics Canada, 2017) for every census year. Crop types with areas of greater than 0.1% of the total county crop area were accounted for in the calculation. The total crop N uptake is the sum of uptake from all crop types.

Table 4. Crop Parameters

Crop Type	Dry matter fraction	N Content fraction	Source
Alfalfa	0.902	0.028	(Hong and Swaney, 2013)
Barley	0.889	0.021	(Hong and Swaney, 2013)
Beans	0.906	0.065	Assumed the same as soybeans
Buckwheat	0.885	0.022	Assumed the same as wheat

Canola	0.906	0.035	(Hong et al., 2012)
Corn for fodder	0.284	0.013	(Hong and Swaney, 2013)
Corn for grain	0.867	0.016	(Hong and Swaney, 2013)
Flaxseed	0.906	0.035	Assumed the same as sunflowers
Hay (non-alfalfa)	0.867	0.013	(Hong and Swaney, 2013)
Mixed grains	0.885	0.022	Assumed the same as wheat
Oats	0.894	0.021	(Hong and Swaney, 2013)
Other Crops	0.223	0.027	Average of all crops
Peas	0.906	0.065	Assumed the same as soybeans
Potatoes	0.223	0.016	(Hong and Swaney, 2013)
Rye	0.881	0.022	(Hong and Swaney, 2013)
Soybeans	0.906	0.065	(Hong and Swaney, 2013)
Sugar beets	0.900	0.023	(Hong et al., 2012)
Sunflowers	0.900	0.035	(Hong et al., 2012)
Tobacco	1.000	0.03	(Hong et al., 2011)
Triticale	0.885	0.022	Assumed the same as wheat
Turnips	0.900	0.016	Assumed the same as potatoes
Wheat	0.885	0.022	(Hong and Swaney, 2013)

The N uptake from pastureland by unconfined livestock grazing on grasses is calculated on a per-head basis via the following equation,

$$GRASS_a = POP_a \times N_{cons,a} \times \frac{1}{3} \quad (15)$$

Where $GRASS_a$ is the N uptake by the grazing livestock type from pastureland [M], POP_a is the population of each grazing livestock type *a* [heads], and $N_{cons,a}$ is the N consumption rate, summarized in **Table 5**. We assume that livestock grazes on pastureland grasses during one-third of the year. The total pastureland N uptake is the sum of grass consumption of all grazing livestock types.

Table 5. Livestock Consumption

Livestock Type (heads)	N Consumption (kg N / head / year)	Source
Beef Cows	102	Hofmann et al., 2006
Dairy Cows	151	Hofmann et al., 2006
Heifers	76	Hofmann et al., 2006
Steers	104	Hofmann et al., 2006
Sheep and Lambs	10.62	Hofmann et al., 2006
Horses and Ponies	59.16	Hofmann et al., 2006

3.3.6. Accounting for non-uniformly distributed crop areas within counties

The mass balance calculations in small subbasins that contain parts of multiple counties may be particularly affected by non-uniform distribution of crops. To disaggregate county level data into a finer scale, we used the Annual Crop Inventory (ACI) database (Agriculture and Agri-Food Canada, 2016a), which contains 30x30m rasters of detailed crop areas for the years 2011 to 2016. We used the ACI's fine scale data in census years (2011 and 2016) to develop an average fraction of cropland from each county within a subbasin. This crop scaling fraction used to correct crop production and BNF calculations for each subbasin for all years.

Table 6. Data sources

Input Data Type		Data	Data Source	Spatial Resolution and extent	Temporal Resolution	Time span
N surplus	**Fertilizer N**	Fertilizer (N)	Table 32-10-0039-01: Fertilizer shipments to Canadian agriculture markets, by nutrient content and fertilizer year, cumulative data	Provincial	Annual	1951 - 2016
	Atmospheric N Deposition	Atmospheric N deposition (wet)	National Atmospheric Chemistry (NAtChem) Data archive and Analysis Facility	Station point data	Annual	1980 - 2011
		Atmospheric N deposition (total)	North American Climate Integration Diagnostics - Nitrogen Deposition Ver. 1 (NACID NDEP-1)	30m gridded, North America	Annual	1860-2013
	Crop N Uptake	Crop specific area	Canadian Census of Agriculture	County	Census years	1911-2016
		Crop specific area (finer)	Annual Crop Inventory	30m gridded, Canada	Annual	2011 - 2016
		Crop specific yield	Table 32-10-0359-01: Estimated areas, yield, production, average farm price and total farm value of principal field crops, in metric and imperial units	Provincial	Annual	1908 - 2017
		Crop nutrient parameters	NANI Accounting Toolbox, Version 3.1.0; Hong et al., 2011; Hong and Swaney, 2013	N/A	N/A	N/A
	Biological N Fixation	Crop Biological N Fixing rates	Hong and Swaney, 2013; Zhang et al., 2016	N/A	N/A	N/A
	Manure N	Livestock	Canadian Census of Agriculture	County	Census years	1901-2016
Domestic waste N		Population	Canadian Census of Agriculture	County	Census years	1901-2016
			Canadian Census	Provincial	Census years	1851-1976
Land Use		Historical crop and pastureland trajectory	Historic Croplands Dataset	0.5 degree gridded, global	Annual	1700 - 2007
			Land Use 1990, 2000 & 2010	30 metres gridded, Canada	Decadal	1990 - 2010
Measured stream data		Stream flow	Canadian Hydrometric Data	Station point data	Daily	1914 - 2016
		Nitrogen concentration	Provincial Water Quality Monitoring Network (PWQMN)	Station point data	Varies: Sub-annual	1965 - 2016
Soil data		Soil porosity, field capacity	Soil Landscapes of Canada (SLC) Ver. 3.2	Varies - Vector polygons based on soil survey data with a scale of 1:1,000,000	N/A	N/A

3.4. Estimation of domestic wastewater production

Domestic waste production was estimated using the Canadian Census of Population (Statistics Canada, 2016c). As summarized in **Table 6**, county level data was used from 1901 to 2016. Prior to 1901, we used the provincial population to estimate county populations. A constant parameter of 5 kg per capita was applied (Hong et al., 2013).

3.5. Estimation of Historical Land use trajectory

To calculate the annual N surplus on cropland, pastureland, and non-agricultural land to as part of ELEMeNT-N's function to retain landscape memory (section 2.3.1), we constructed a historical trajectory of land use that spanned from 1700 to 2016 for each of the subbasins. To do this, we used the Annual Crop Inventory (Agriculture and Agri-Food Canada, 2016a), which had data from 2011 to 2016, supplemented with the Historical Croplands Dataset developed by Ramankutty and Foley (1999) that contained modelled estimates of global cropland and pastureland area fractions for each year from 1700 to 2007, with a resolution of 0.5 degrees. To retain continuity between the two datasets, the Historical Croplands Dataset was scaled to the Annual Crop Inventory, using a scaling factor calculated from 2007 values from the Historical Croplands Dataset and 2011 values from the Annual Crop Inventory, since there was no change in cropland fraction from 1990 to 2010 (Agriculture and Agri-Food Canada, 2015). The resulting trajectory for the GRW is shown in **Figure 5**.

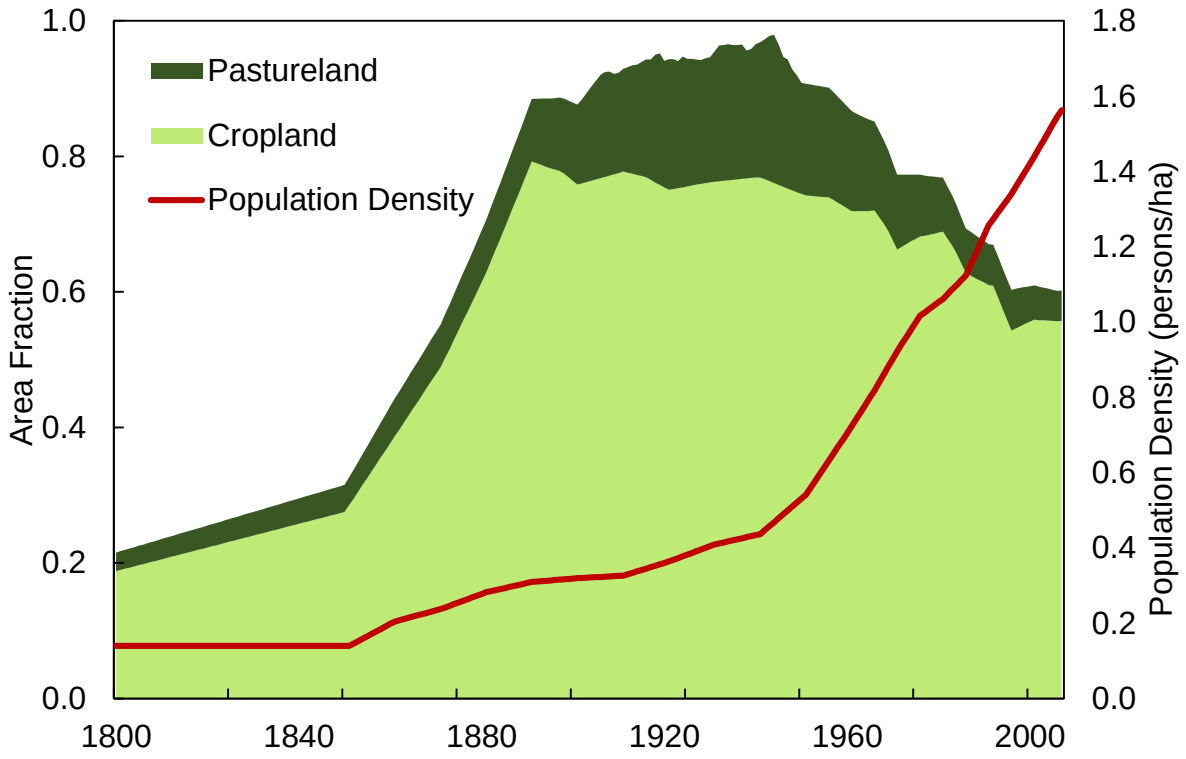

Figure 5. Land use and human population trajectories for the GRW. Cropland and pastureland trajectories are from Canada Open Government's Annual Crop Inventory, supplemented by historical modelled cropland data from Ramankutty and Foley (1999), aggregated to the watershed scale.

3.6. Estimation of Flow-weighted concentrations

To estimate annual stream N loads, we used a method called Weighted Regressions on Time, Discharge, and Season (WRTDS) using the EGRET software package (Hirsch and Cicco, 2015; Hirsch et al., 2010). Daily stream flow data was typically available, but concentration data generally had only 6 to 12 data points per year. WRTDS estimates daily concentration values using daily flow data and the available concentration data via the following equation:

$$\ln(c) = \beta_0 + \beta_1 t + \beta_2 \ln(Q) + \beta_3 \sin(2\pi t) + \beta_4 \cos(2\pi t) + \varepsilon \quad (16)$$

Where c is the concentration [M/L^3]; β_0 through β_4 are fitted regression coefficients; Q [L^3/T] is daily stream flow; t [T] is time, and ε is an error term.

Error metrics of the WRTDS estimations for the 14 basins are summarized in below,

Table 7. WRTDS Error Metrics

Subbasin	Flow Station ID	Water Quality Station ID	MBE	MAE	RMSE	NSE	PBIAS (%)	Sample count
Canagagigue Creek	2GA023	16018401602	-0.021	1.218	1.755	0.570	-0.47	527
Conestogo River	2GA028	16018407702	0.156	0.767	1.097	0.501	5.64	357
Whitemans Creek	2GB008	16018410602	-0.041	0.651	1.051	0.461	-1.05	376
Nith, New Hamburg	2GA018	16018403202	-0.095	1.023	1.563	0.547	-3.10	439
Nith, Canning	2GA010	16018400902	-0.074	0.645	1.062	0.653	-2.41	500
Eramosa River	2GA029	16018410202	0.003	0.232	0.346	0.580	0.28	367
Speed, Armstrong	2GA040	16018409902	0.009	0.252	0.350	0.659	0.66	301
Speed, Guelph	2GA015	16018403402	0.075	0.258	0.438	0.548	6.45	387
Grand, Marsville	2GA014	16018406702	0.003	0.216	0.397	0.624	0.52	379
Grand, Shand Dam	2GA016	16018403702	0.050	0.277	0.461	0.465	6.33	502
Grand, West Montrose	2GA034	16018410302	-0.014	0.497	0.747	0.531	-0.80	307
Grand, Galt	2GA003	16018401002	-0.015	0.489	0.697	0.682	-0.54	544
Grand, Brantford	2GB001	16018402402	0.025	0.515	0.773	0.639	0.86	471
Grand, York	2GAC06	16018409202	-0.023	0.524	0.705	0.653	-0.79	324

Using the estimated daily concentration, we calculated the flow-weighted mean concentration (FMC) analysis using the following equation:

$$FWMC = \frac{\sum_i^n (c_i q_i)}{\sum_i^n (q_i)} \quad (17)$$

Where i is the index of daily samples, n is the total number of samples, c_i is the concentration in the i-th sample, t_i is the time interval for i-th sample (1 day), and q_i is the flow in the i-th sample.

The annual stream N loading was also calculated using the daily discharge and WRTDS concentration estimates.

3.7. Parameter data: Soil

We obtained data on current soil characteristics from the Soil Landscapes of Canada database of soil polygons (Agriculture and Agri-Food Canada, 2016b). The database contained data for different soil layers in the first 1m of the soil profile. We extracted current levels of soil organic carbon by calculating an area and depth weighted average for the GRW and each of its subbasins. To estimate soil organic nitrogen content, we used a carbon to nitrogen conversion factor of 14 (Cleveland and Liptzin, 2007). The current soil organic nitrogen estimation is used as a model calibration point, described in section (3.6.3). We also extracted other soil properties for analysis, including hydraulic conductivity and soil texture.

3.8. Sensitivity Analysis and Model Calibration

We conducted a sensitivity analysis to select model parameters for optimization. The model was calibrated using the optimization tool OSTRICH to optimize the simulation of (1) current levels of SON, and (2) N loading at the catchment outlet. We adopted a sequential calibration methodology for nested subbasins. In the following sections, we describe the methodology for data collection for parameter range estimation (3.8.1), sensitivity analysis (3.8.2), model output datasets for calibration (3.8.3), and sequential calibration methodology (3.8.3).

3.8.1. Parameter range estimation

Ideally, all parameters used for calibration are constrained using observed data as they carry a considerable amount of uncertainty. Unfortunately, site-specific data was unavailable for most parameters. We first set reasonable parameter ranges centred around values informed by available data or previous studies to conduct a sensitivity analysis. Then we further constrained ranges of parameters that were found to be sensitive. The parameters that had data and previous studies to aid in determining a preliminary range were the pristine SON content (M_s), soil porosity (n), soil water content (s), and mean travel time (μ). For M_s estimates, we used data from Zinke et al.'s (1998) Global Organic Soil Carbon and Nitrogen database to inform a range for calibration. Zinke's carbon estimates were converted to nitrogen using a carbon to nitrogen conversion factor of 14 (Cleveland and Liptzin, 2007). We extracted other soil parameters, porosity (*n)* and soil water content (*s*), from the Soil Landscapes of Canada database using the same methodology described in section (3.7) (Agriculture and Agri-Food Canada, 2016b). Note that field capacity, defined as soil water retention at -33 kPa, was used as a proxy for *s*. The upper limit for μ was set based on Van Meter and Basu's (2017) estimates of lag times in the GRW using cross-correlation analysis between annual NANI and annual FWMC of nitrate. Otherwise, ranges from Van Meter et al.'s (2017) calibration of ELEMeNT for the Mississippi River Basin were used for sensitivity analysis, which were determined based on literature review and knowledge of the watershed. The final sensitivity analysis parameter ranges are summarized in **Appendix A**.

3.8.2. Sensitivity Analysis

We conducted a global parameter sensitivity analysis to identify model parameters that have the most significant influence on soil organic N (SON) content and stream N loading for the GRW at the Grand at York station (Mishra, 2009; Muleta and Nicklow, 2005; Van Meter et al., 2017). We used a stepwise regression analysis to test the sensitivity of all potential parameters for calibration simultaneously. We identified 10 parameters that we could potentially calibrate (**Appendix A**). We used the Latin Hypercube Sampling technique, a form of stratified Monte-Carlo sampling, to generate the input variables of the analysis by randomly sampling each parameter across its respective range with uniform distribution (Muleta and Nicklow, 2005; Van Meter et al., 2017). The resulting input variables consisted of 1000 unique parameter sets. We ran model simulations using these parameter sets and extracted output variables consisting of the residual sum of squares values of (1) mean annual stream N loading, 1977 to 2016; and (2) median SON content, 1950 to 2016. The output variables were rank transformed to account for nonlinearities in the model (Iman and Conover, 1979; Van Meter et al., 2017). We carried out the stepwise analysis using these input-output pairs for the annual stream N loading and the SON content. Results of the stepwise regression analysis are shown in **Table 10**. We chose the most sensitive parameters for calibration and fixed the values of the parameters that the model was not sensitive to by using best estimates, to minimize computation time.

3.8.3. Model Calibration and Validation

The sensitivity analysis was used to select model parameters for optimization. The model was calibrated to optimize the simulation of (1) current levels of SON, and (2) N loading at the catchment outlet. Median SON levels for the watersheds were calculated based on the Soil

Landscapes of Canada database of soil polygons (Agriculture and Agri-Food Canada, 2016b). Catchment N loading data for the 14 basins were calculated using the weighted regression on time, discharge and season method (WRTDS) (Hirsch et al., 2010) using the EGRET software package (Hirsch and Cicco, 2015). Three separate objective functions were used for model calibration: (1) maximizing the Kling-Gupta Efficiency (KGE) metric between the modelled and measured N loading (Gupta et al., 2009), (2) minimizing the percent bias (PBIAS) between the modelled and measured N loading and (3) minimizing the PBIAS between the modelled and measured SON levels:

$$KGE = 1 - \sqrt{(CC - 1)^2 + \left(\frac{\sigma_s}{\sigma_m} - 1\right)^2 + \left(\frac{\mu_s}{\mu_m} + 1\right)^2} \quad (18)$$

where *CC* is the Pearson correlation coefficient between the simulated and measured N loading time series; σ_s and σ_m are the standard deviation of the simulated and measured time series, respectively; and μ_s and μ_m and are the means of the simulated and measured time series, respectively,

$$PBIAS_{NLoad} = \frac{\sum Q_m - Q_s}{\sum Q_m} \times 100 \quad (19)$$

where Q_m and Q_s are the annual measured and simulated N loadings, and

$$PBIAS_{SON} = \frac{SON_m - SON_s}{SON_s} \times 100 \quad (20)$$

where SON_m and SON_s are the measured and simulated SON content, respectively. Note that the SON_m is not a time series but rather an estimate of the SON content in the year 2011 (Agriculture and Agri-Food Canada, 2016b).

We used OSTRICH, a model-independent optimization tool that has multi-objective optimization capabilities, for model calibration (Matott, 2017). Within the OSTRICH platform, the Pareto-Archived Dynamically Dimensioned Search (PA-DDS) algorithm was chosen for its multi-objective optimization capabilities, its simple implementation, and design to find acceptable solutions rather than globally optimal solutions (Asadzadeh and Tolson, 2013; Tolson and Shoemaker, 2007). The PA-DDS algorithm works by generating parameter sets (solutions) globally across the allowed parameter ranges at the beginning of the search, and dynamically and probabilistically focusing on perturbing fewer paramters as the iterations approaches the user specified maximum number of iterations. With each iteration, PA-DDS archives (retains) the set of non-dominated solutions, and generates a new canadidate solution by taking one of the non-dominated solutions, and perturbing randomly selected parameters by a randomly sampled magnitude from a normal distribution with a mean of 0. If the candidate solution is dominating or non-dominated compared to the archived set solutions, it is archived and randomly perturbed in the next interation. If the new candidate solution is dominated however, another non-dominated set is selected for perturbation in the same iteration (Asadzadeh and Tolson, 2013). Using the PA-DDS algorithm for model calibration, a large number of unique parameter sets that are optimized to our objective functions can be generated.

The calibration time frame for annual stream loading was from 2000 – 2016, and the validation time frame was from 1965 to 1999. Exceptions were made for subbasins, particularly the Speed below Guelph, which did not have stream concentration data from 1997 to 2006. In this case, the

calibration timeframe was from 1990 to 2016, and the validation timeframe from 1965 - 1989. The modelled SON level in 2011 was calibrated to measured soil N levels.

Each parameter in the headwater subbasins was given a range for constraining perturbation in OSTRICH's calibration algorithm. When possible, the ranges were informed by data and given a stricter range if it was a sensitive parameter, such as for the pristine SON content (M_s). The final parameter ranges used for calibration are summarized in **Table 8**. We ran five separate OSTRICH runs of 200 iterations, with each run having a random initial value for each parameter, and each interation varying the parameter values across this range. Out of the 1000 parameter sets that were generated from OSTRICH, we selected for acceptable parameter sets if the 3 model performance metrics used as calibration objective functions met the acceptance criteria. The acceptance criteria were: (1) KGE of stream N loading equalling or exceeding 0.5, (2) absolute PBIAS of stream N loading not exceeding 10%, (3) and absolute PBIAS of SON content not exceeding 25%. To account for nested subbasins, headwater basins were calibrated first, followed by downstream subbasins. The parameter calibration for the headwater basins were allowed to be varied by the full range listed in **Table 8**, and accepted parameter sets were retained, based on the acceptance criteria. The accepted parameter ranges of the upstream basins were then used for calibrating the downstream basins. This was done to ensure that a relationship along the river continuum is retained.

Table 8. Calibration Ranges for parameters in headwater basins

Parameter	Lower bound	Upper bound	Reference
$\mathbf{M_s}$	7250	8750	Zinke et al., 1998
$\mathbf{k_a}$	0.09	0.17	Van Meter et al., 2017b
$\boldsymbol{\lambda}$	0.25	0.75	Van Meter et al., 2017b

$\mathbf{h_c}$	0.14	0.26	Van Meter et al., 2017b
$\mathbf{h_{nc}}$	0.28	0.75	Van Meter et al., 2017b
μ	3	34	Van Meter et al., 2017a,b
γ	0.07	0.13	Van Meter et al., 2017b
$\mathbf{k_h}$	0.56	0.85	Van Meter et al., 2017b

3.9. Comparing calibrated travel times with watershed attributes

Groundwater travel time distributions (TTD) have been estimated for watersheds using a GIS-based approach using soil property data and Darcy's Law (Schilling and Spooner, 2006). It is a relatively accessible method of estimating travel times, with comparable results to complex numerical models (Basu et al., 2012). We compared the calibrated μ with the mean travel time (TT) estimated from the GIS-based approach to explore relationships in the ELEMeNT-N parameters and observed landscape characteristics.

We estimated mean TT using the GIS soil type methodology using the method described by Basu et al., (2012). A digital elevation map was used to calculate the slope gradient *i*, while soil porosity *n*, and hydraulic conductivity *K*, were extracted from the Soil Landscapes of Canada database (Agriculture and Agri-Food Canada, 2016b) (Section 3.7). The flow length *L* of each cell is the number of cells separating it and the nearest stream, multiplied by the cell width. A stream network was created using a 40.5 ha accumulation threshold. First, the landscape was divided into a 30x30m raster with gridded data for elevation, *i*, *n*, and *K*. Then, the travel time for each cell was calculated based on Darcy's Law for saturated flow, expressed as the following equation:

$$t = \frac{L}{v} = \frac{nL}{Ki} \quad (21)$$

Where *t* is cell travel time, *L* is flow path length, *n* is soil porosity, *K* is hydraulic conductivity, and *i* is the slope gradient calculated as the difference in elevation over distance.

All GIS operations were done in QGIS 3.

3.10. Uncertainty in input and output estimations

It should be noted that for estimations in N surplus, annual stream loading, and model parameters, there are uncertainties associated with the values. In N surplus calculations, uncertainties arise from the values of the unit conversion parameters from the studies cited, as well as uncertainties in the census collection data. Past mass balance studies have characterized the uncertainty using monte carlo simulations to give these estimations an upper and lower boundary (Mishra, 2009; Van Meter et al., 2017). In this study, we have not performed uncertainty characterization of these parameters as it is not the focus of the thesis, but instead used the best estimates we have, though it would be beneficial to do an uncertainty analysis in the future. For measured stream loading, there are large uncertainties due to the low temporal resolution of stream concentration measurements used for loading calculation. We used WRTDS to mitigate this uncertainty, and although there are also uncertainties associated with the WRTDS outputs, its estimates of daily concentrations greatly minimize the uncertainties of average stream concentration at an annual scale. Finally, uncertainties associated with the model calibration parameters are characterized by using an acceptable range of parameters through the calibration method.

Chapter 4 Results and Discussion

The following sections describe the results of applying ELEMeNT to subbasin scale catchments to explain the controls of legacy N behaviour across a heterogeneous landscape. We first examine the historical N surplus trajectory of the GRW and 13 of its subbasins (Section 4.1), and then examine its relationship with the flow-weighted N concentrations in the stream. We developed ELEMeNT for all 14 basins, and present sensitivity analyses and model calibration and validation results (Section 4.2 - 4.3). We also examine the variation in the calibrated parameter sets between subbasins that allows for ELEMeNT to capture the effects of landscape heterogeneity across the GRW (Section 4.4). Finally, we show the modelled trajectories of legacy pools, and reveal possible drivers of where legacy N accumulates in the landscape (Section 4.5).

4.1. Historical Trends of Nitrogen Sources and Sinks in the GRW

4.1.1. Nitrogen Surplus and its Components

We developed trajectories of N surplus and its components for the 14 subbasins in the GRW for the time period between 1800 and 2016. **Figure 6a** shows the trajectories beginning in the year 1900, when significant changes to the N surplus trend occurred for the GRW and all its subbasins. The temporal pattern of the trajectories is similar across the subbasins, with N surplus < 10 kg/ha/yr until the 1950s, followed by a rising trend starting in the 1950s and peaking in the late 1980s, with magnitudes more than 7 times greater than those in the pre-1950s (**Figure 6a**, Table 7). From the late 1980s to the 2000s, N surplus declined by 9% to 25%. Interestingly, since the 2010s, the N surplus appears to be rising again. This is most likely caused by an

increase in fertilizer application that has been observed across Canada, including Ontario (Dorff and Beaulieu, 2014; Statistics Canada, 2016b) .

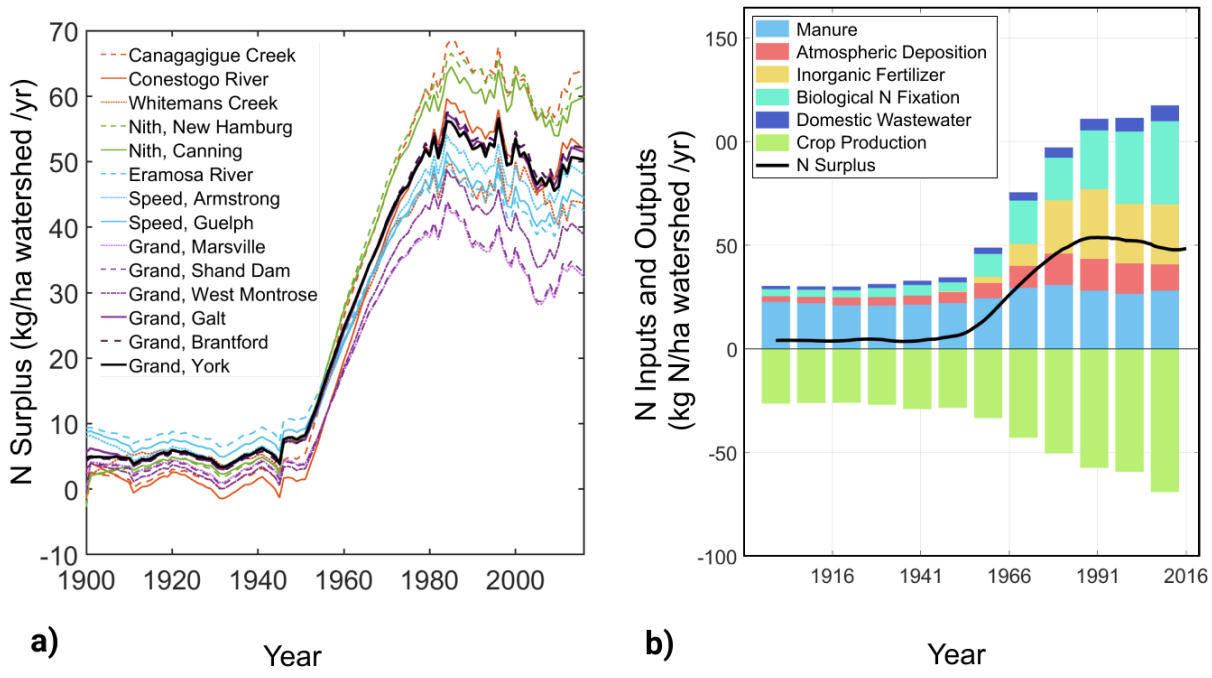

Figure 6. N Surplus Trajectories: (a) Surplus trajectories of the GRW (Grand at York) and its 13 subbasins, (b) Surplus component plot describing the contribution of inputs and outputs to the surplus

Although the temporal patterns in the N surplus trajectories are similar between the subbasins, the magnitude of the N surplus varies significantly across the GRW **(Figure 6a)**. The 1980s peak N surplus varies from a low of 43 kg/ha/year in the Marsville subbasin to a high of 69 kg/ha/year in the Canagagigue subbasin **(Figure 6a)**. The lower N surplus in the Marsville subbasin can be attributed to its low proportion of agricultural area (48% agricultural land from 2006 – 2016 (Agriculture and Agri-Food Canada, 2016a; Ramankutty and Foley, 2007)), while the higher N surplus in the Canagagigue subbasin can be attributed to its larger proportion of agricultural area (~71%). Marsville also has the highest density of wetlands in the GRW, accounting for 20% of

its area (Grand River Conservation Authority, 2016, 2008). The subbasins with the highest N surplus, Canagagigue Creek, Conestogo River, and the Nith subbasins, all had the highest proportions of agricultural land use in the GRW, averaging 71% to 76% in the last 10 years. These subbasins have greater N surplus than other less agriculturally developed subbasin, such as the Speed and Eramosa Rivers (41% to 55%). The Grand at York averages across these agriculturally intensive and non-intensive basins and thus shows an intermediate N surplus.

Table 9. N surplus Peaks and Troughs using a 10-year moving average to identify peaks and troughs in N surplus

	1800 to 1950 baseline (kg N/ha)	Peak Magnitude	Peak Year	Peak to Baseline Ratio
Canagagigue Creek	1.4	65.0	1988	45.3
Conestogo River	1.4	55.9	1988	39.9
Whitemans Creek	3.7	46.4	1999	12.5
Nith, New Hamburg	1.5	63.5	1988	41.6
Nith, Canning	2.3	61.3	1988	26.2
Eramosa River	6.9	47.3	1984	6.9
Speed, Armstrong	5.7	50.8	1988	8.9
Speed, Guelph	6.3	48.4	1985	7.7
Grand, Marsville	2.0	40.4	1984	20.6
Grand, Shand Dam	1.8	40.9	1984	22.3
Grand, West Montrose	2.8	45.5	1985	16.1
Grand, Galt	4.7	54.2	1988	11.5
Median	**3.3**	**51.5**	**1988**	**14.6**
Min	**1.4**	**40.4**	**1984**	**6.9**
Max	**6.9**	**65.0**	**1999**	**45.3**

The components of the N surplus trajectory for the entire GRW is shown in **Figure 6 (b)**. Overall, N surplus in the current years is dominated by BNF, followed by manure, fertilizer, atmospheric deposition and human waste. This is in contrast to the pre-1950s N surplus, where manure is the largest N input, followed by BNF, while fertilizer contribution is relatively small. The post-WWII economic boom brought about rapid industrialization in the region, fueled by fossil fuels, and the widespread use of chemical N fertilizer (Duinen, 2008). There was also a shift towards growing N fixing crops like soybeans and alfalfa (Bowley, 2013). The domestic waste component also increased from previous decades due to the rapidly growing urban centres, though its relative magnitude is small at the watershed scale compared to other components. By the late 20th century, the N Surplus trend started to plateau. This is attributed to improved crop production efficiency as a result of advancements in fertilizer application methods and higher yielding crops (**Figure 6 (b)**) (Lassaletta et al., 2014).

The N surplus component trajectories for the subbasins generally follow the same trends as the GRW as a whole **(Figure 7)**, though the extent of crop, pasture, and urban land vary across the subbasins. The higher N surpluses in the intensive agricultural subbasins, such as the Canagagigue, Conestogo, and Nith, are driven by higher fertilizer application rates combined with high BNF that arose from the dominance of N fixing cash crops such as soybean and alfalfa (**Figure 7a, c**). Trends in fertilizer N application (**Figure 7a**) are parallel to the observed trends in N surplus across all subbasins **(Figure 6a)**, with a rising trend since the 1950s, peaking in the 1980s, declining till 2000s, and then increasing after 2010 **(Figure 7a)**. BNF also had a rapid growth phase in all subbasins in the 1950s, catalysed by stimulated demand for soybeans during WWII **(Figure 7b)** (Bowley, 2013). In the decades following the 1950s, BNF doubled in 30

years from 1970 to 2000, from 15 kg/ha/year to 29 kg/ha/year in the Eramosa River as the lower bound, and 23 to 49 kg/ha/year in the Canagagigue Creek as the upper bound. The rise in BNF rates can be attributed to increased soybean cultivation as the crop became more popular due to its high yield varieties and resilience to pests and disease (Bowley, 2013). There was a sharp drop in BNF in 2001 **(Figure 7b)**, which was caused by a pan-Canadian drought (Wheaton et al., 2008). The drought severely reduced yields of the GRW's major crops that fix N, such as soybeans and hay (including alfalfa) (Wheaton et al., 2008). After the drought, BNF rates quickly recovered and reached higher rates than ever before, ranging from 30 to 60 kg/ha across the GRW. Crop production reflects much of the same trends seen in BNF, though crop production started to increase earlier, in the 1940s **(Figure 7c)**. The rising adoption of specialized crop farming, use of fertilizer, and continuously improving crop yields due to advancements in farming technology allowed crop production to stay on an upwards trend since (Bowley, 1996). It is evident that the 2001 drought that affected BNF also had a significant impact on overall crop production. It not only diminished soybeans and hay production, but also corn for grain, another major field crop (Statistics Canada, 2016a; Wheaton et al., 2008).

Manure N application rates are relatively homogeneous with no trend across the subbasins, and averaging ~ 22 kg/ha/yr between 1900-1950 **(Figure 7d)**. Application rates increased post 1950 due to increasing demands for dairy products in the post-war economy (G. R. Smith, 2015). Between 1950-1976, manure production rates became heterogeneous across the GRW, with rates ranging from 22 to 42 kg/ha/year across the subbasins by 1976. After 1976, manure production rates decreased, or are relatively flat across most watersheds except Canagagigue Creek that had increased manure production. The Grand at Marsville, Shand Dam, and West Montrose had 8 to 10 kg/ha/yr less manure production in 2016 than its peak in 1976, since dairy production became

more efficient per head of cow, and demand for dairy products dropped since the late 1970s (G. R. Smith, 2015).

The atmospheric deposition pattern is uniform across the GRW, which rose steadily since the early 20th century and plateaued by the 1970s between 15 to 18 kg/ha/year due to increased industrial combustion processes **(Figure 7e)** (Hember, 2018). After 1990, there was a noticeable declining trend in atmospheric N deposition consistent with results attributed to reduction policies such as the Canada-US Air Quality Agreement (Zbieranowski and Aherne, 2011).

Finally, domestic waste production has been steadily rising in all subbasins since the mid 19th century as a reflection of population growth **(Figure 7f)**. While domestic waste production rates were relatively homogeneous across the GRW from 1900 – 1950 (mean = 1.25 kg N/ha/yr, standard deviation = 0.65 kg N/ha/yr), heterogeneity started emerging post 1950, as a function of spatial patterns of urban development. In the most recent decade from 2006 - 2016, domestic waste production had a mean of 5.5 kg N/ha/yr with a standard deviation of 3.4 kg N/ha/yr.

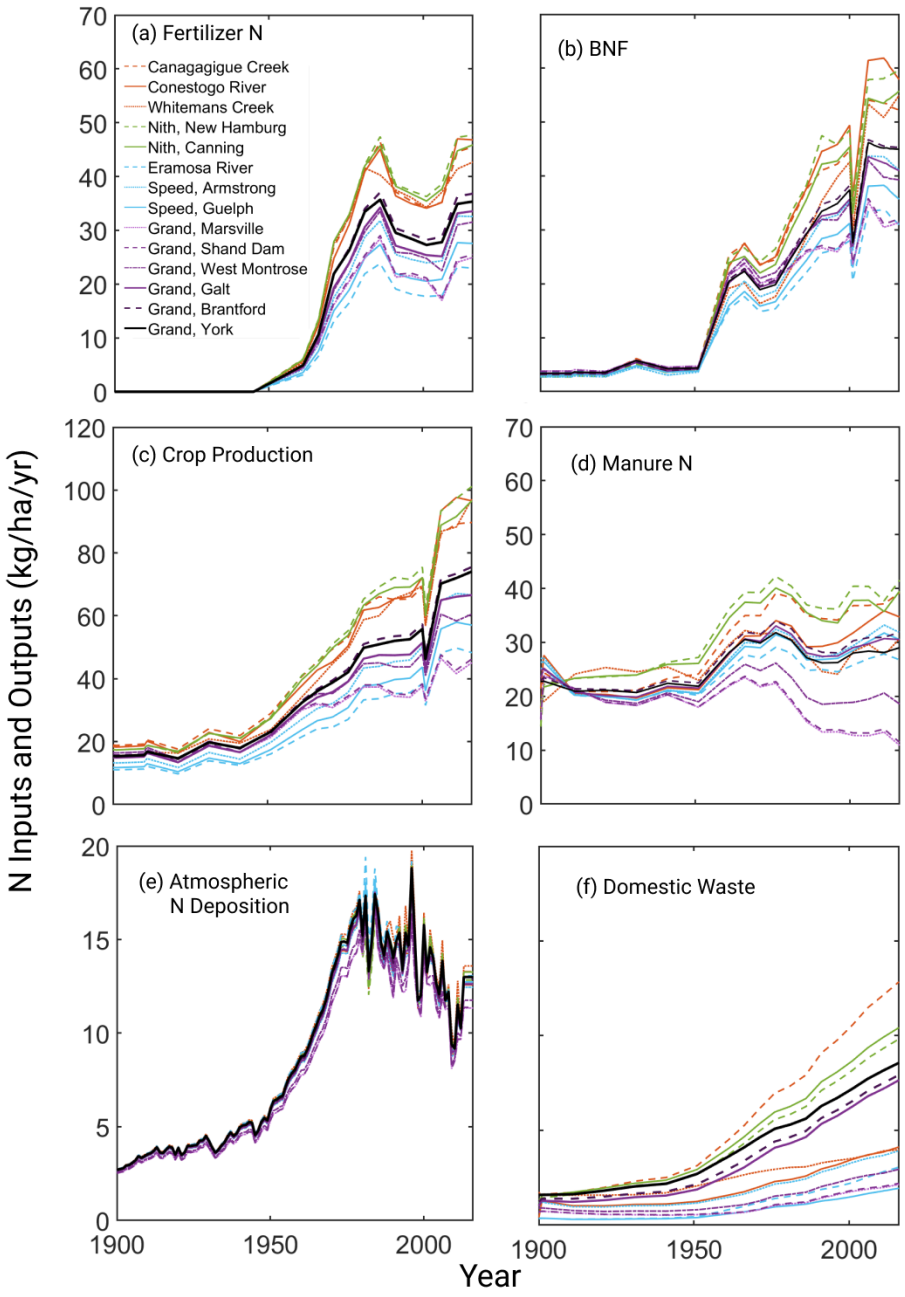

Figure 7. Components of the N surplus trajectory from 1900 to 2016 in each subbasin. The N surplus input components are (a) Fertilizer N, (b) BNF, (d) Manure N (e) Atmospheric Deposition, and (f) Domestic Waste. The output from the N surplus calculation is (c) Crop Production.

4.1.2. Temporal relationship between N surplus trajectories and stream N loads

We further examined trends in N export from subbasins and their relationship with N surplus over time **(Figure 8)**. As mentioned in Section 4.1, the N surplus for all the subbasins in the GRW rose from 1950 to 1980 and declined across the GRW until the late 2000s. The flow-weighted mean concentrations (FWC) followed the increasing N surplus trends from the 1950s to 1980s. Afterwards, the concentration trends in the subbasins began to diverge, and can generally be categorized into 2 types of trends, (1) Category 1: FWC peaked sometime after N surplus peaked in 1980 and has been declining since then, (2) Category 2: FWC has been monotonically increasing over time **(Figure 8)**.

Category 1 is most dominant and include 11 of the 14 basins: the Canagagigue Creek, Conestogo River, Whitemans Creek, the Nith at New Hamburg and at Canning, Eramosa River, Speed at Armstrong and Guelph, Grand at Brantford, West Montrose, and Grand at York **(Figure 8a-h, k,m,n**). The rates of increase and decrease and the peak timing is variable across basins. Of these, the subbasins that show the greatest magnitude of decline after peak **(Figure 8a-e)** are the agriculture dominated basins in the West of the GRW, with agriculture accounting for 71% – 76% of its land use in 2006 to 2016 (Agriculture and Agri-Food Canada, 2016a; Ramankutty and Foley, 2007). They are also the subbasins with the highest tile drainage density in the GRW, ranging from 27% - 55% due to the poorly drained till soils. The rising FWC limb is related to the increasing N surplus, and the disconnect between the timing of N surplus and FWC peaks is a reflection of time lags of the system. Interestingly, although the FWC at the Conestogo River fell from 2000 to 2010, it appears to be increasing again in the 2010s, following the slight increase of N surplus. The Eramosa, Speed River at Armstrong and below Guelph also belong to this first category **(Figure 8g, h).** However, the rising and falling limbs, and the peak at these subbasins

are much less pronounced. The Eramosa and the Speed at Armstrong flow into the Speed below Guelph, and these are two of the less agriculturally developed subbasins (47% - 55%). They have relatively low N surplus inputs, accompanied by low FWCs. The Speed has sandy soils (>50%, (Agriculture and Agri-Food Canada, 2016b)) and the Paris-Galt moraine that are credited with the good water quality of the subbasins (Loomer and Cooke, 2011). Finally, the Grand at Brantford, West Monrose and at York are the other subbasins that show a peak, followed by a declining FWC trend. These are more downstream stations along the Grand, and their signal is a function of the upstream subbasins that contribute to their N load. FWC in the Category 2 subbasins, Grand at Marsville, Shand Dam, and Galt **(Figure 8i, j, l),** have been monotonically increasing over time. Marsville and Shand Dam are located in the Northern till plains, and have the highest wetland densities in the GRW (18.5% - 20% (Grand River Conservation Authority, 2016)). In contrast to the first category, Category 2 subbasins have relatively low agricultural development (48 – 49%) and low tile drainage density (9%). There is also a major reservoir between the Marsville and Shand Dam subbasins. All of these factors lend to long lag times (Van Meter and Basu, 2017).

The decoupling between N surplus and stream loading is related to the differences in land use development (e.g., tile drain installation, reservoir construction, and wastewater treatment plant operation) that determine whether current or legacy N is released to streams (Van Meter and Basu, 2017). To uncover the causes of this variability more explicitly, we used a modelling approach to find the spatially varying controls on N export across the watershed.

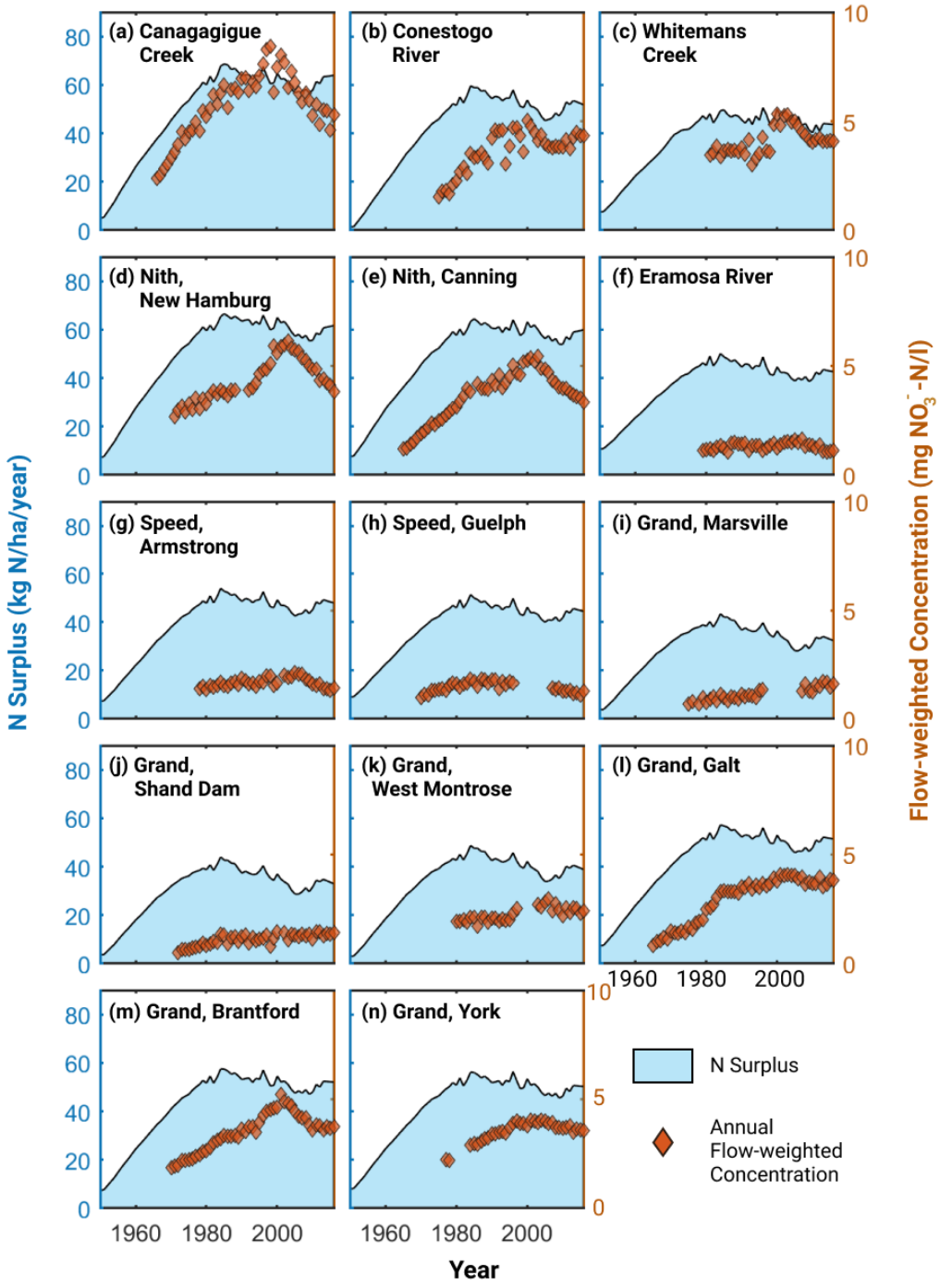

Figure 8. **Surplus trajectory compared with flow-weighted mean concentration** for 14 modelled basins (a-n). The distance between peaks in watershed surplus and peaks in concentration is an indication of the lag time for N export in the subbasin.

4.2. Model Calibration and Validation

The N surplus trajectories and its components were used as inputs into the ELEMeNT-N model to simulate N loading for the 14 subbasins of the GRW **(Table 1)**. Sensitivity analysis for the Grand at York showed that the primary parameters affecting N loading at the catchment outlet were denitrification rate constants in soil and groundwater (γ and λ), and the mean travel time (μ) through the subsurface pathways **(Table 10)**. In contrast, the 1950 to 2016 median SON levels are primarily impacted by pristine nitrogen content (M_s), mineralization rate of active SON (k_a), and protection coefficient of cultivated land (h_c). This is similar to the ELEMeNT models developed for the Mississippi and Susquehanna basins in the US (Van Meter et al., 2017). The outputs extracted from the stepwise regression analysis is reported in **Table 10**.

Table 10. Parameter sensitivity results for mean stream N loading (1977 – 2016) and median SON content (1950 – 2016)

Parameters	**Mean stream N load (1977 – 2016, available years)**			**Median SON (1950 - 2016)**		
	Step Number	**absolute SRC**	**p-value**	**Step Number**	**absolute SRC**	**p-value**
M_s	-	0.000	0.602	1	1.000	0.000
k_a	6	0.036	<0.000	2	0.024	0.000
n	-	0.000	0.082	-	<0.000	0.640
s	-	0.000	0.333	-	<0.000	0.208
λ	3	0.474	<0.000	-	<0.000	0.483
h_c	5	0.057	<0.000	4	0.008	0.000
h_{nc}	7	0.033	<0.000	3	0.019	0.000
μ	2	0.528	<0.000	-	<0.000	0.169
γ	1	0.587	<0.000	-	<0.000	0.840
k_h	4	0.270	<0.000	-	<0.000	0.775

The modelled and measured time trajectories of N loads for GRW and its 13 subbasins are shown in **Figure 9.** The model was calibrated from 2000 to 2016 and validated from 1965 to 1999, except the Speed below Guelph. Parameter sets were accepted during the calibration period if they met the criteria for KGE ≥ 0.5 for modelled stream N loading, PBIAS ≤ 10% for stream N loading, and PBIAS ≤ 25% for SON content. This resulted between 512 to 811 parameter sets for each subbasin. The best parameter set for each subbasin was then chosen based on the highest calibrated stream N loading KGE from within the accepted parameter sets. We found the best parameter set to range between KGE of 0.67 to 0.95 **(Table 11),** where 1 indicates a perfect model reproduction of measured loads, and -0.41 indicates that the model predicts as well as the mean of the observed loads (Knoben et al., 2019). These parameter sets were then run over the validation time frame, and the KGE for the validation timeframe for the best runs ranged from 0.57 to 0.89 across the 14 basins. The calibration PBIAS of the best chosen parameter sets ranged from 0.2% to 10%, while the PBIAS of the validation time period was larger and ranged from -24% to 39%. Of the nine subbasins that had PBIAS values > 10% in the validation timeframe, three basins were under-predicted **(Figure 9g, h)** while six of them were over-predicted (16% to 39%). One of the reasons for poorer prediction in the validation time frame arises from non-stationarity in the parameter space. We assume the model parameters to be constant in time, however, parameters like the mean travel time can vary over decadal time frames due to land management practices like installation of tile drains. In the next paragraph, we explore how this alters our model predictions in the validation time period.

Subbasins that were over-predicted in the validation timeframe with PBIASs exceeding 20% included Conestogo River, Grand at Marsville, Shand Dam, West Montrose, and Galt. Over-prediction in these basins, however, was not consistent across the calibration/validation

timeframes. Specifically, the over-predicting subbasins appear to consistently over-predict prior to a specific change point **(Figure 9b, i-l)**. We hypothesized that the over-prediction indicated that calibrating to the 2000 – 2016 timeframe did not capture the different hydrologic conditions of the early timeframe due to the recent increase in tile drainage. Increasing tile drain density over the years would contribute to shortening the mean travel time. Thus, using the later period's mean travel time to the earlier period was contributing to an under-estimation of travel time in the earlier period -- shorter travel times indicate lower denitrification and greater N loads, and thus, the over-prediction.

Table 11. Error metrics of median model output trajectory for all modelled subbasins

	Stream N Loading						SON content
	KGE		NSE		PBIAS		PBIAS
	Calibration	Validation	Calibration	Validation	Calibration	Validation	Calibration (2011)
Canagagigue Creek	0.67	0.73	0.81	0.79	6%	-13%	6%
Conestogo River	0.84	0.65	0.81	0.66	8%	23%	17%
Whitemans Creek	0.95	0.77	0.91	0.62	0%	16%	4%
Nith, New Hamburg	0.95	0.84	0.92	0.83	1%	6%	3%
Nith, Canning	0.91	0.89	0.85	0.96	4%	4%	3%
Eramosa River	0.94	0.86	0.88	0.70	1%	-4%	3%
Speed, Armstrong	0.93	0.57	0.47	0.23	2%	-24%	0%
Speed, Guelph	0.81	0.71	0.69	0.31	9%	-22%	3%
Grand, Marsville	0.83	0.57	0.70	-0.54	6%	39%	19%
Grand, Shand Dam	0.86	0.70	0.73	0.45	3%	21%	20%
Grand, West Montrose	0.85	0.67	0.86	-0.32	10%	26%	13%
Grand, Galt	0.84	0.71	0.67	0.71	2%	23%	< 0.0%
Grand, Brantford	0.91	0.88	0.83	0.89	2%	9%	5%
Grand, York	0.85	0.81	0.88	0.93	9%	3%	10%

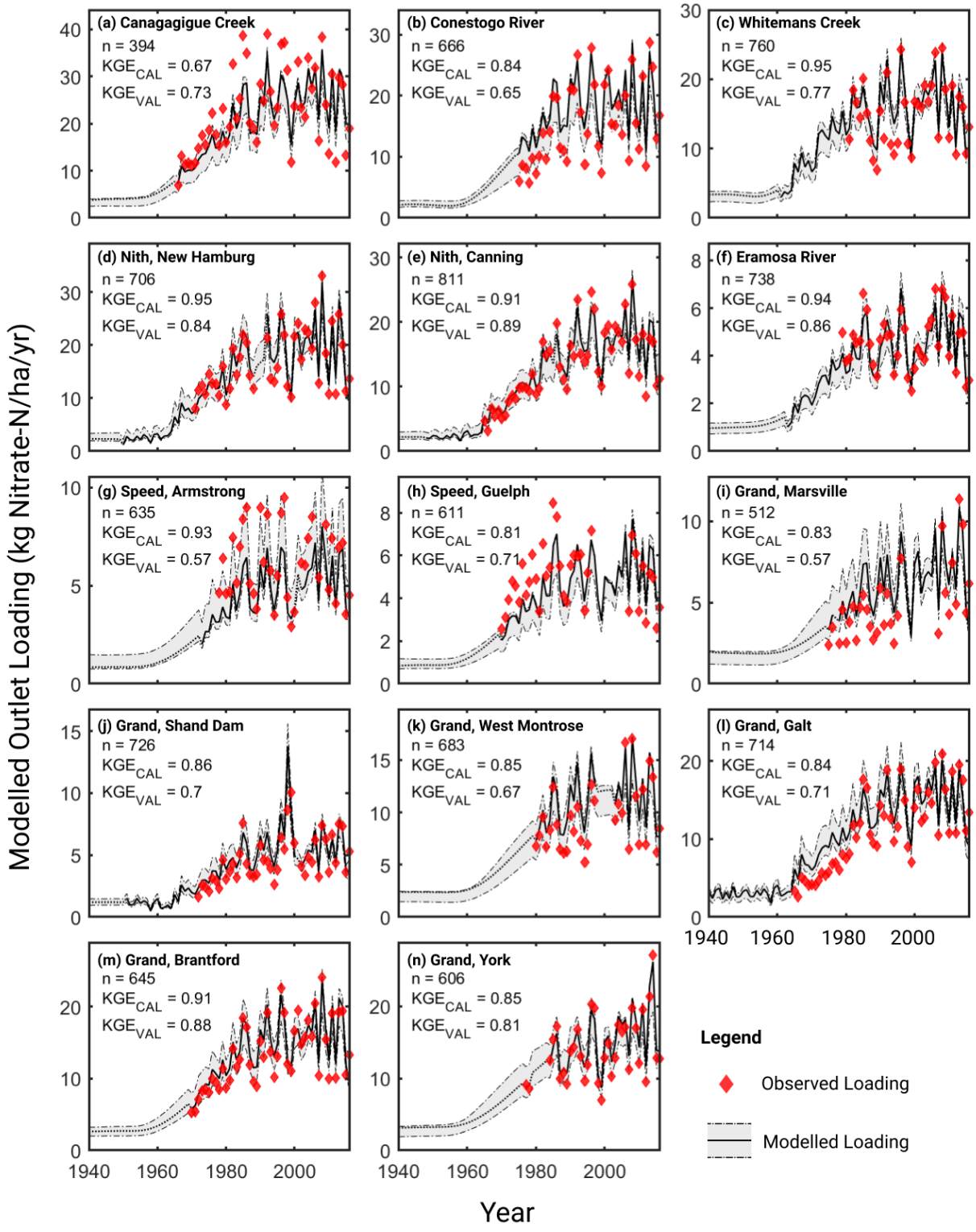

Figure 9. **Modelled and measured stream loading** for 14 modelled basins (a-n)

Unfortunately, the tile drain density map that is available is a current dataset, and there is no information on how this has evolved over the years. To address this issue, we followed the work of Foufoula-Georgiou et al. (2015) to define Land-Cover Transition (LCT) as the point in time at which the area under row crops exceeded that of hay and small grains. It has been argued that conversion of small grains to row crops is accompanied by extensive tile drain installation, given the different soil moisture requirements of the two crop types (Bajgain et al., 2015; Hobbs and Muendel, 1983; Oosterhuis et al., 1990). The area of corn exceeded that of hay and small grains at different points in time within these five watersheds **(Appendix B)**. We used OSTRICH to calibrate for μ value in the time period before the LCT, using the best calibrated parameter set for all other parameters. The calibrated μ in the pre-LCT time period were longer, representative of less tile drainage, and resulted in a better model fit **(Table 12, Figure 13)**.

Table 12. Comparison of model performance metrics on stream N loading employing a temporally varying μ in the pre-LCT timeframe

	μ (years)		**KGE**		**NSE**		**PBIAS (%)**	
	Preliminary Calibrated μ	**pre-LCT μ**	**Preliminary Calibrated μ**	**pre-LCT μ**	**Preliminary Calibrated μ**	**pre-LCT μ**	**Preliminary Calibrated μ**	**pre-LCT μ**
Conestogo River	5.8	11.7	0.62	0.79	0.28	0.90	33%	1%
Grand, Marsville	23.3	33.4	0.57	0.85	-0.54	0.79	39%	8%
Grand, Shand Dam	14.8	20.4	0.54	0.60	0.22	0.48	24%	4%
Grand, West Montrose	11.8	16.2	0.64	0.79	-0.59	0.51	25%	7%
Grand, Galt	5.1	7.5	0.62	0.65	0.52	0.74	29%	14%

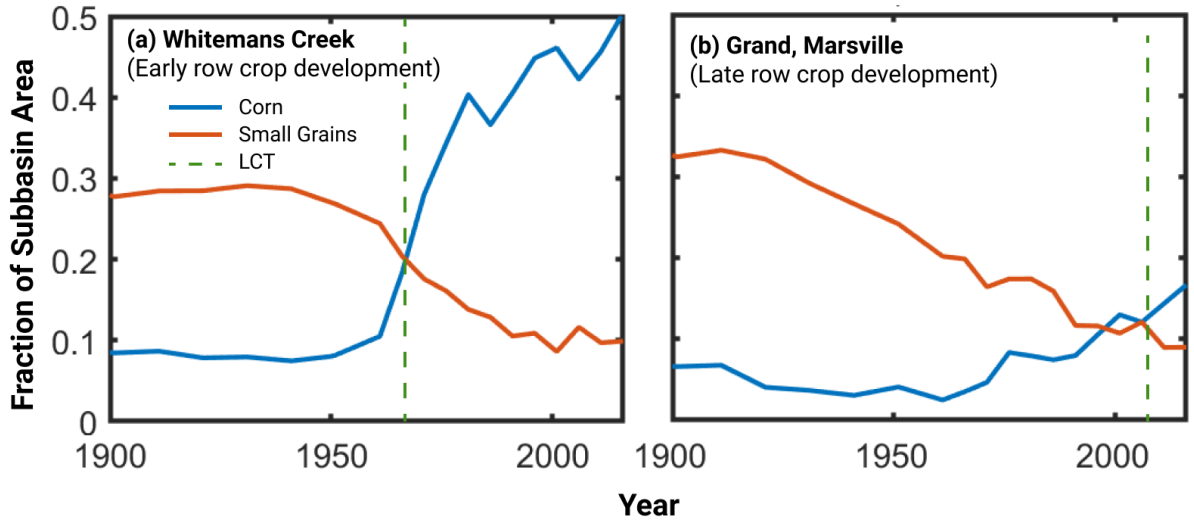

Figure 10. **Examples of Land-Cover Transition** in (a) an early developed subbasin and (b) a late developed subbasin

4.3. Modelled stream N loading trajectories

The ELEMeNT framework allows us to estimate the long-term, historical N loadings from each modelled subbasin in a landscape that is continuously evolving in a non-uniform way. The model outputs give an estimation of the baseline stream N loading in the period prior to monitoring efforts for N constituents. The modelled NO_3-N loading trajectories from 1940 to 2016 for all of the subbasins in the GRW is shown in **Figure 9**. The baseline loading for all subbasins can be seen in the period before 1945, where the loading trend is flat. According to the model, the 10-year mean baseline average from 1935 to 1945 ranges from 0.9 kg/ha/year (Eramosa River) to 3.5 kg/ha/year (Canagagigue Near Elmira). Higher baseline N surplus magnitudes occurred in subbasins that were first developed for agriculture by European settlers. After this period, almost all of the subbasins experienced an increasing trend in stream N fluxes until they peaked in 2005

or 2010, with the exception of Shand Dam, which peaked earliest in 1995. The beginning of the rising trend in the loading corresponds with the rise in N surplus components, including N fertilizer use, manure production, and BNF, but the peak loading is later than that of the N surplus (**Figure 6 &Figure 7**).

Table 13. 10-Year Moving Average Peaks of Modelled Stream N Load Trajectories

	1935-1945 baseline (kg N/ha)	10-year moving average peak year	10-year moving average peak (kg N/ha)	10-year moving average peak : baseline ratio
Canagagigue Creek	3.5	2009	25.4	7.3
Conestogo River	2.2	2005	19.1	8.5
Whitemans Creek	3.1	2005	18.0	5.8
Nith, New Hamburg	2.6	2005	21.5	8.3
Nith, Canning	2.4	2005	18.0	7.5
Eramosa River	0.9	2010	5.3	5.8
Speed, Armstrong	1.2	2010	7.3	6.3
Speed, Guelph	0.9	2010	5.6	6.0
Grand, Marsville	1.5	2010	7.5	5.0
Grand, Shand Dam	1.2	1995	7.0	5.7
Grand, West Montrose	1.9	2005	11.6	6.3
Grand, Galt	2.6	2005	16.4	6.2
Grand, Brantford	2.7	2010	17.3	6.4
Grand, York	2.9	2010	16.9	5.9

4.4. Spatiotemporal Patterns in the Calibrated Travel Time

The disconnect between the very similar N surplus trajectories, and the very different stream N loading trajectories across the various subbasins in the GRW, can be attributed to landscape heterogeneity that might be natural or management-driven.

4.4.1. Spatial patterns in the Mean Travel Time

The calibrated mean of our exponential travel time distribution (μ) varied across the GRW (**Figure 11**), from 5 years at the Canagagigue Creek and 6 years at Whitemans Creek to 15 years at the Grand River at Shand Dam and 31 years at the Eramosa River. We explored the relationship between μ and % silt and clay in the watershed **(Figure 12a)**, the saturated hydraulic conductivity **(Figure 12b)**, and the GIS derived mean travel time **(Figure 12c)**. Against conventional wisdom, there appeared to be a negative correlation between μ and % clay, and a positive relationship between μ and the saturated hydraulic conductivity, indicating that travel times are shorter in less permeable, clayey soils **(Figure 12a)**. Indeed, we found a negative correlation between the GIS estimated travel time based on Darcy's Law, and the calibrated μ **(Figure 12c)**. We hypothesized that this occurs due to human management and alteration of the natural landscape, where regions with high clay content and low hydraulic conductivities **(Figure 12b)** are also areas that are heavily tile drained. This led to a decoupling of the relationship of a subbasin's effective travel time and the groundwater travel time estimated based on Darcy's Law. We tested our hypothesis by comparing the calibrated μ of the 7 headwater basins with the extent of tile drainage **(Figure 12d)**. The strong, negative correlation of μ and fractional tile drained area ($R^2 = 0.75$, $p = 0.01$) proves that indeed travel times are lowered in regions with tile drains. The relationship indicates that the calibration was able to capture the

behaviour of effective hydrological flow in modelled subbasins. The presence of tile drains can alter the travel time of a subbasin by short-circuiting subsurface flow where travel times are longer (Schilling et al., 2012).

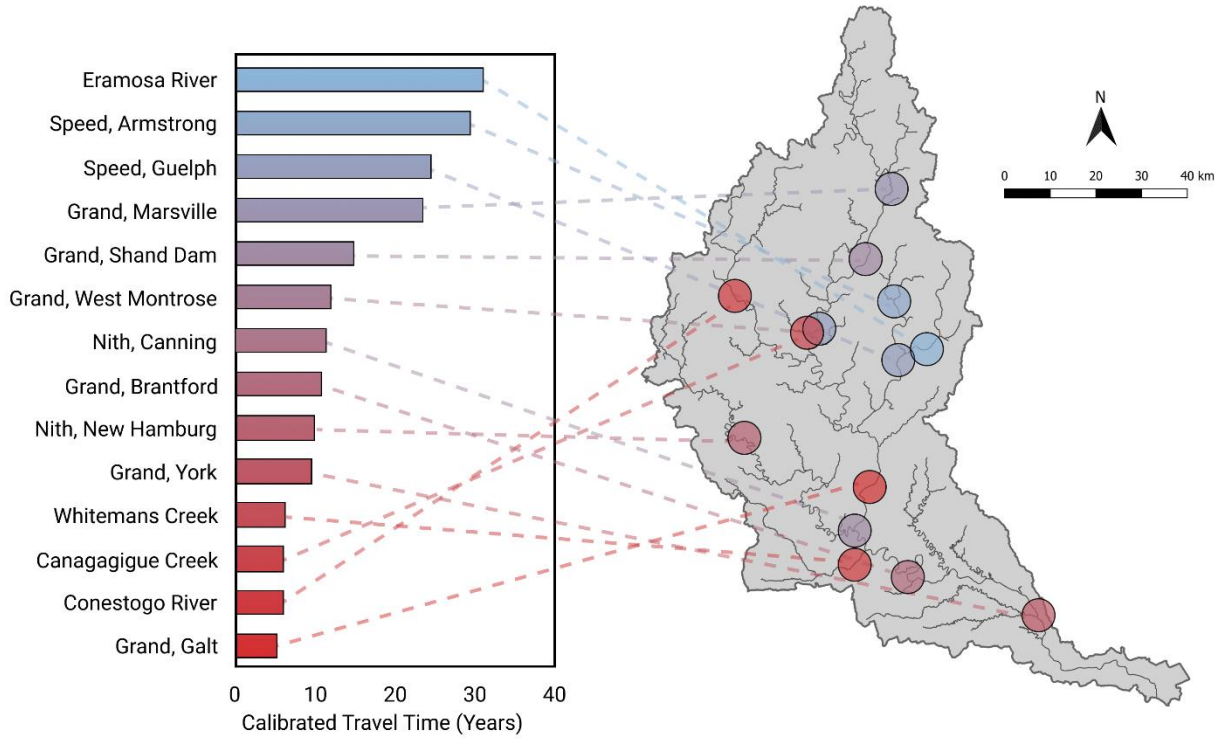

Figure 11. Calibrated mean travel time of modelled subbasins

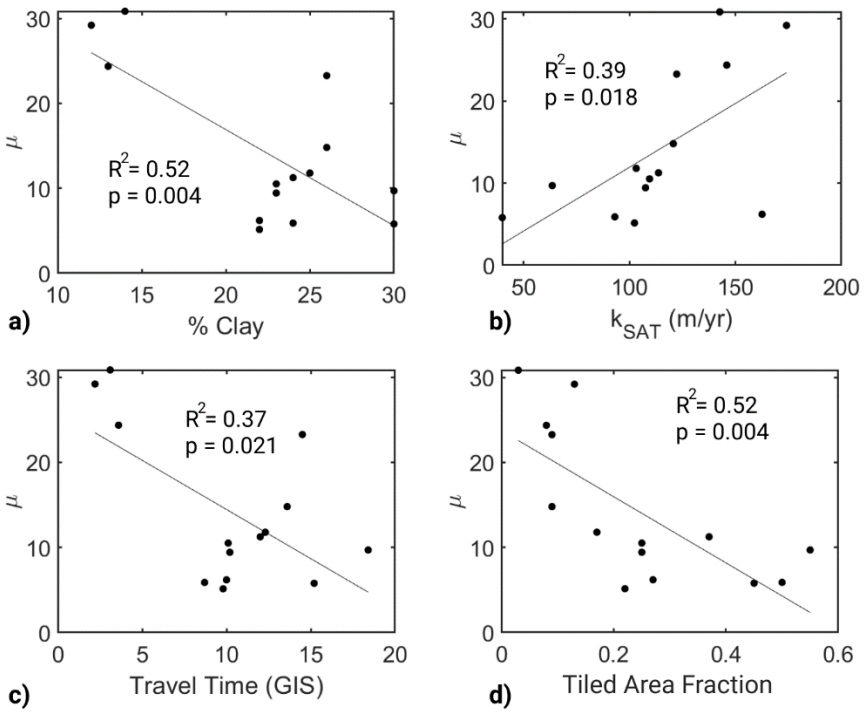

Figure 12. Correlation analysis of calibrated mean travel time (μ) with landscape characteristics showing (a) percent clay vs μ, (b) hydraulic conductivity vs μ, (c) GIS Travel time vs μ, and (d) tiled area fraction vs μ.

4.4.2. Temporal Patterns in the Mean Travel Time

The strong dependence of the calibrated μ on the % tile-drained area highlights the strong management controls on nitrogen legacies and time lags. However, it also raises a question on the validity of the use of a single travel-time distribution over the years. Tile drain density has changed over time, and this is likely to contribute to a decrease in the mean travel time in these watersheds. To explore this effect, we re-calibrated the μ in the earlier time period by keeping everything else constant, but allowing only the μ to vary. We found that indeed pre-LCT μ were longer than post-LCT μ, indicating that increase in tile drainge in these subbasins has contributed to a short-circuiting of flow pathways. We then wanted to see the effect of such short-circuiting

on stream N loads. To do this, we ran the model in the later time period, but with the pre-LCT travel times. We found that indeed N loads in the stream has increased between 5% for the larger basins like the Grand at Brantford, to 26% for smaller subbasins like the Grand at Marsville. It is known that the effect of tile drains is more dominant at smaller scales.

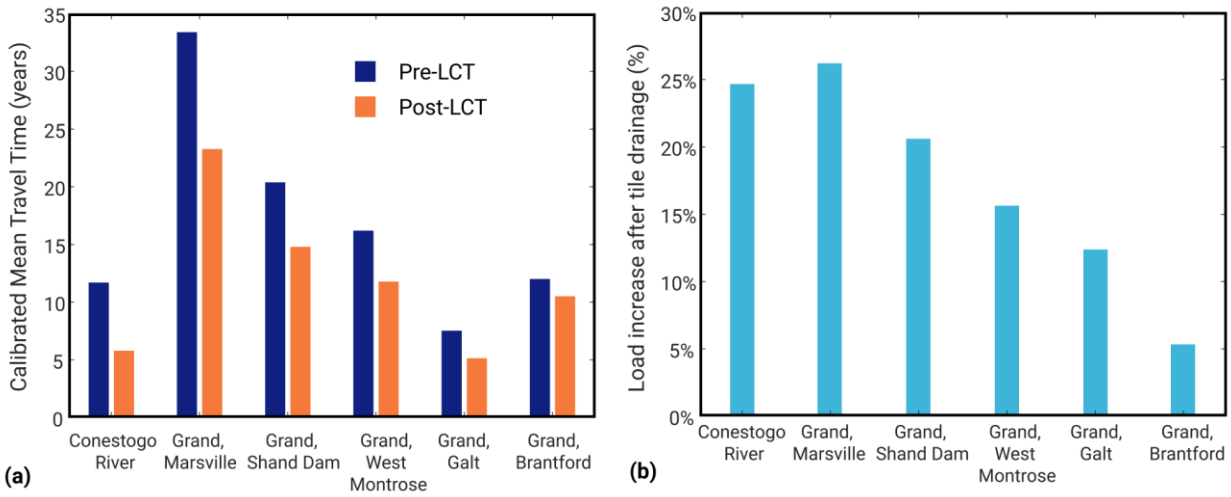

Figure 13. Comparison of modelled μ and loading in (a) pre- and (b) post-Land Cover Transition (LCT)

4.5. Nitrogen Fluxes and Stores along the River Continuum

4.5.1. The Fate of the Missing N

Over the last 76 years (1940 to 2016) across the GRW the cumulative N surplus amounted to 2875 kg/ha **(Figure 14)**. This N surplus can leave the system as stream N fluxes, landscape denitrification (soil and groundwater), and WWTP denitrification, or accumulate within the system as soil organic N or within the groundwater system. These pools and fluxes are impossible to assess without using a modelling framework like ELEMENT. Across the GRW, we find that only 26% (10 kg/ha/yr over the timeframe) of the cumulative N surplus was exported from the watershed through the stream, while denitrification in WWTPs, soil, and

groundwater accounted for 30% (11 kg/ha/yr) of the N surplus. This leaves 44% of the N surplus stored on the landscape as legacy N since 1940 (17 kg/ha/yr) **(Figure 14a)**. Of this, majority (55%) is stored in the soil, while 45% is stored in the groundwater **(Figure 14a)**.

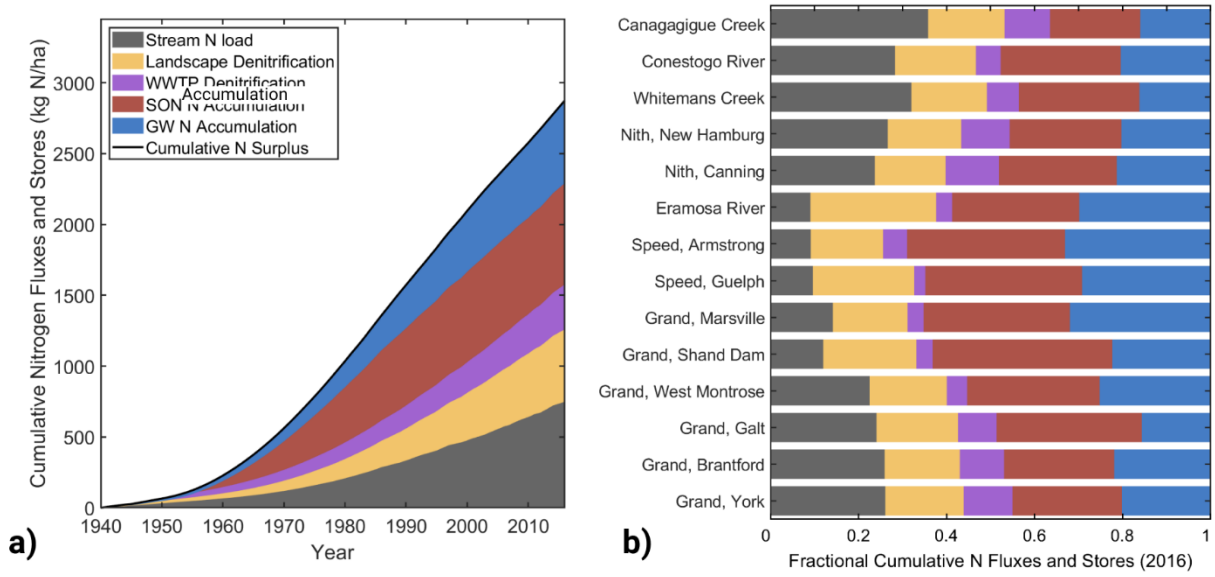

Figure 14. Fate of Missing N since 1940 showing (a) Cumulative N fluxes and stores in the GRW (at York) and (b) in 14 modelled basins

The proportions of these fluxes and stores vary across the GRW **(Figure 14b)**. We find that in subwatersheds across the GRW 9% to 36% of the cumulative N surplus is exported from the watershed through the stream, while denitrification in WWTPs, soil, and groundwater accounted for 21% to 32% of the N surplus. This leaves 37% - 69% of the N surplus stored on the landscape as legacy N since 1940 **(Figure 14b)**, 49% to 68% of this is stored in the soil, while 32% to 51% is stored in the groundwater **(Figure 14b)**. Higher proportion of stream N load is apparent in the heavily tile drained and agricultural watersheds like the Canagagigue Creek, Conestogo River, Whitemans Creek, and the Nith basins, while watersheds with significant wetland coverage (Grand at Marsville, wetland coverage = 20%) have a lower proportion of

stream N load. The latter group of watersheds also have a much higher proportion of SON and groundwater N accumulation than the tile drained watersheds.

The effect of reservoirs is apparent when examining three stations: (1) Grand at Marsville and below Shand Dam, that are upstream and downstream of the Belwood reservoir, and (2) Speed, Guelph that is downstream of the Guelph Lake. In the Grand at Marsville and Grand at Shand Dam pair, the proportion of N exported from the downstream station is lower than the N exported from the upstream station **(Figure 14b)**. Also, the downstream station has higher proportions of denitrification flux than the upstream one. The higher denitrification flux and lower stream N load can be attributed to dam effects. The Speed, Guelph does not have an analogous upstream station, but the effect of reservoir denitrification is apparent in the higher proportion of the denitrification flux **(Figure 14b)**. Both the Shand Dam and Guelph Dam reservoirs can develop anoxic conditions in the hypolimnion, particularly during warm temperatures, allowing denitrification to occur (Baets, 2016; Mackie et al., 1983).

It is also notable that the Speed and Eramosa Rivers have large proportions of their N lost to denitrification compared to other subbasins. These subbasins are some of the least developed, with only 3% of the area covered by tile drainage in the Eramosa to 8% in the Speed at Guelph, 41% to 47% of the land used for agriculture, have one of the lowest N surpluses, and no major wastewater treatment plant discharging upstream of the subbasin outlets. As a result, the Speed and Eramosa Rivers have some of the best water quality in the GRW with low stream N concentrations (Loomer and Cooke, 2011). The high proportion of N loss through denitrification can be attributed to the subbasin's high forest cover and resulting SOC due to reforestation efforts in the 1950s (Grand River Conservation Authority, 2008; Mitchell and Shrubsole, 1992).

Next, we examined the variability in the magnitude of groundwater N accumulation and SON content of each subbasin across the GRW (**Figure 15)**. The box plots show the modelled ranges of the magnitudes of the biogeochemical and hydrologic legacy accumulated from 1900 to 2016 in each subbasin. The median estimates of the SON accumulation in the different tributaries of the GRW vary from 760 kg/ha to 950 kg/ha, and groundwater accumulation ranges between 320 kg NO_3^--N/ha to 675 kg NO_3^--N/ha. Estimates for groundwater accumulation have a wider confidence interval than that of SON, with the largest confidence interval occurring in the Speed at Armstrong, with a range of 250 to 950 kg NO_3^--N/ha. This wide confidence interval demonstrates the high uncertainty of groundwater estimates and that the availability of groundwater data is important for tightening this range of uncertainty.

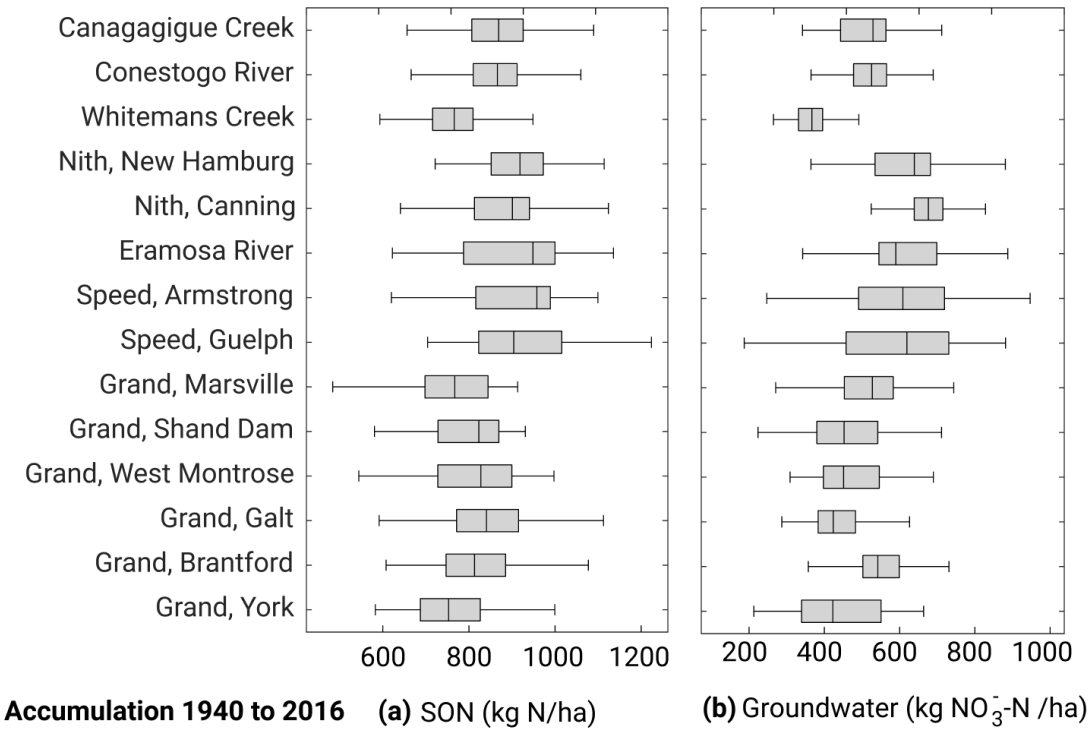

Figure 15. Area normalized nitrogen legacy magnitudes since 1940 in 14 modelled basins showing (a) SON, and (b) groundwater N

We hypothesized that under the dramatic N surplus regime shift as the result of the rise of agriculture after 1900, N surplus became a stronger driver of N dynamics in the watershed. It appears however, that in **(Figure 15)**, the subbasins with high tile drainage and agricultural activity such as Canagagigue Creek, Conestogo River, Whitemans Creek, and the Nith basins do not have the highest legacy accumulation. To expand our analysis into SON accumulation, we analyzed the accumulation of active SON in particular. We found that there was a significant relationship between net magnitude of active SON and N surplus, indicating that the surplus is contributing to the build-up of active SON **(Figure 16a)**.

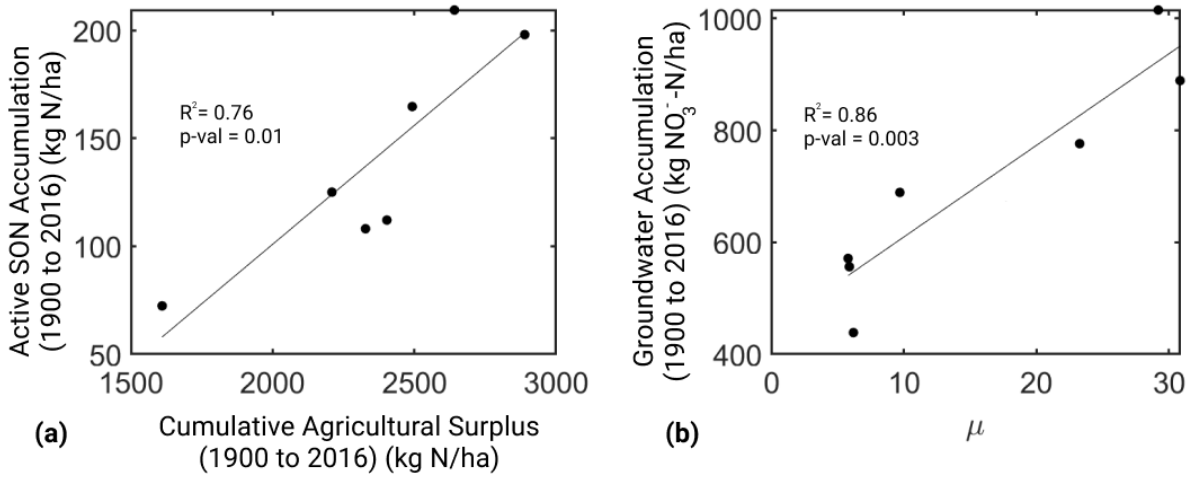

Figure 16. Drivers of (a) active SON and (b) groundwater N accumulation

On the other hand, groundwater accumulation does not appear to be driven by N surplus (R^2 = 0.08 , p = 0.547). Groundwater N accumulation is instead driven by the calibrated mean travel time parameter, μ **(Figure 16b)**. Interestingly, although μ is strongly correlated with intensive agricultural landscapes with soil texture and tile drainage **(Figure 12a,d)**, there is no relationship between groundwater N accumulation and either characteristic individually (R^2 = 0.42, p =

0.114; $R^2 = 0.42$, p = 0.115). As SON and groundwater N accumulation have different controls, the result is a patchwork of the type and magnitude of legacy across the GRW (**Figure 17**).

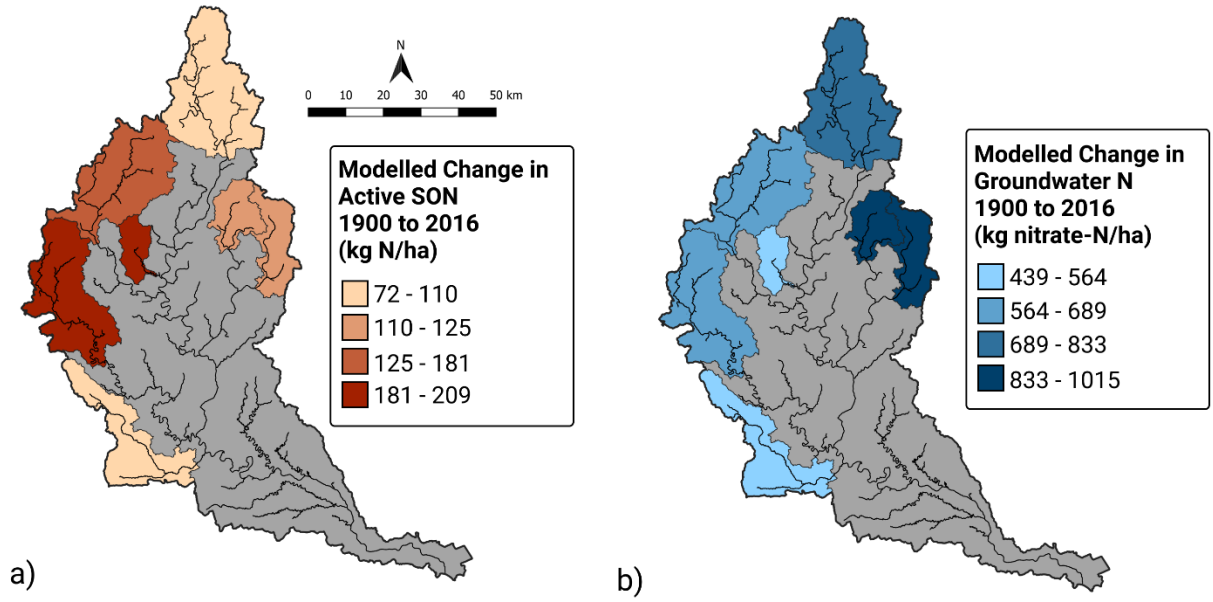

Figure 17. **Map of legacy accumulation** in the 7 headwater basins since 1900, showing (a) SON and (b) groundwater N

Chapter 5 Conclusion

5.1. Summary

The objectives of the thesis were to create a long-term mass balance trajectory of N for the GRW at the subbasin scale, use a process based model, ELEMENT, to quantify legacy stores and accumulation trajectories over the last 200 years, and to find drivers of legacy accumulation and their associated lag times. We used as a case study, the Grand River Watershed, a 6800 km2 agriculturally-dominated watershed, and developed models for 7 headwater subbasins, and 7 more subbasins along the main stem.

We found that the N surplus across the GRW dramatically increased after 1950 and peaked in 1980 ranging from 39 kg/ha to 58 kg/ha. This growth in N surplus was primarily due to high rates of BNF from soybeans and hay cultivation. Across the watershed, high yielding crops and better fertilizer use efficiency led to a steady decline in the peak until the 2010s, illustrating that improvements in N management are effective in reducing N surplus. The flow-weighted N concentration increased with increase in N surplus, but showed a lagged response in the peak behavior.

We found that the calibrated mean travel time can range widely across the GRW, from 5 to 31 years, and strongly depends on the presence of tile drainage. Regions with greater density of tile drainage show shorter travel times. The stores of legacy N in the watershed has been steadily accumulating since 1950. On the other hand, the size of the biogeochemical legacy in the form of SON is significantly and positively correlated to the cumulative surplus and current fraction of cropland.

5.2. Implications and Future Work

Our findings have significant implications with respect to watershed management to minimize lag times and reach water quality targets for nutrients, specifically nitrogen, in agricultural watersheds. First, we must consider the effects of biogeochemical legacy and groundwater N accumulation have on stream water quality in the long-term. Targets designed to reduce stream loading by reducing N at the source do not account for the slow release of N from SON, and the long travel times of N in groundwater to the stream. Depending on physical characteristics of the watershed, the lag time between implementation of nutrient management practices and visible improvements in stream water quality can span decades under the most rigorous N reduction scenarios (Ilampooranan et al., 2019; Van Meter et al., 2018). In the GRW alone, mean travel times can be up to 31 years (Eramosa River). Thus, we recommend that lag times due to legacy be considered when designing water quality targets to ensure they are feasible.

Second, we can tailor management practices to local legacy problems. Currently, agricultural best management practices are often applied in a blanketed or 'one-size-fits-all' approach. Without acute understanding of specific nutrient problems in a region, BMP adoption may not achieve desired outcomes. By identifying the location and the dominant type of legacy accumulating, we can prioritize the adoption of more effective nutrient management practices. For example, in a subbasin such as the Canagagigue with high N surplus, and high SON accumulation, cover crops could effectively reduce stream N loading by minimizing leaching to groundwater. In contrast, in an area with long mean travel times, such as the Eramosa River, leached N can build up groundwater N. In this case, reducing the N surplus by improving N uptake efficiency and waiting for the N to be flushed out of the system would be the long term choice. However, in the short term it might be necessary to construct wetlands that can intercept

groundwater N and improve water quality faster. Thus, we recommend that the appropriate BMP is implemented where benefits offer good returns of investment, and develop long-term plans that are prepared for reasonable lag times to observable improvements in stream water quality.

Finally, we can optimize management resources further by prioritizing subbasins with the shortest time lags for best management practice implementation. This strategy would theoretically lead to the fastest and greatest improvement in stream water quality (Van Meter and Basu, 2015). By prioritizing subbasins that have elevated levels of active SON and short groundwater travel times, such as in Nith at New Hamburg and Canagagigue Creek, we may be able to achieve some short term water quality targets (Van Meter and Basu, 2015). Having measurable success in management efforts can boost morale and encourage continued funding for long term water quality improvements. Such targeting strategies would theoretically result in the fastest and greatest response in stream N loading, and offer evidence for continuing long-term nutrient management plans needed for sustained water quality improvements.

While we made estimates of legacy accumulation in soil and groundwater pools, and identified some drivers, there is more work to be done to refine our findings. First fo all, we currently do not have any data to validate legacy accumulation. It may be possible to validate these estimates should data become available. Future work could involve obtaining well nitrate data, and deep soil core data to validate and refine accumulation estimates should such datasets become available. We have also suggested the practical implications of our findings for targeted nutrient management policies. To support the viablility of the recommendations, we will need to simulate future scenarios of targeted BMP implementation strategies to quantify potential short and long-term improvements in water quality. Finally, this thesis was focused on nitrogen legacy, but ELEMeNT has been developed to model phosphorus dynamics at the watershed scale as well

(Van Meter et al., *in-review*). We can run ELEMeNT for phosphorus at the subbasin scale for the GRW to explore similarities and differences of drivers of legacy P accumulation, and reveal any dual-nutrient benefits of targeted management strategies.

References

Agriculture and Agri-Food Canada, 2016a. Annual Crop Inventory.

Agriculture and Agri-Food Canada, 2016b. Soil Landscapes of Canada.

Agriculture and Agri-Food Canada, 2015. Land Use 1990, 2000 & 2010.

Allinger, L.E., Reavie, E.D., 2013. The ecological history of Lake Erie as recorded by the phytoplankton community. Journal of Great Lakes Research 39, 365–382. https://doi.org/10.1016/j.jglr.2013.06.014

Asadzadeh, M., Tolson, B., 2013. Pareto archived dynamically dimensioned search with hypervolume-based selection for multi-objective optimization. Engineering Optimization 45, 1489–1509. https://doi.org/10.1080/0305215X.2012.748046

Baets, B.J.D., 2016. Effects of Hydroelectric Dams on Downstream Oxygen and Nitrogen in the Grand River and Conestogo River.

Bajgain, R., Kawasaki, Y., Akamatsu, Y., Tanaka, Y., Kawamura, H., Katsura, K., Shiraiwa, T., 2015. Biomass production and yield of soybean grown under converted paddy fields with excess water during the early growth stage. Field Crops Research 180, 221–227. https://doi.org/10.1016/j.fcr.2015.06.010

Basu, N.B., Jindal, P., Schilling, K.E., Wolter, C.F., Takle, E.S., 2012. Evaluation of analytical and numerical approaches for the estimation of groundwater travel time distribution. Journal of Hydrology 475, 65–73. https://doi.org/10.1016/j.jhydrol.2012.08.052

Beeton, A.M., Edmondson, W.T., 1972. The Eutrophication Problem. Journal of the Fisheries Research Board of Canada 673–682.

Behrendt, D.H., Huber, P., Kornmilch, M., Opitz, D., Schmoll, O., Scholz, G., Uebe, R., 2000. Nutrient Emissions into River Basins of Germany 14.

Beniston, J.W., DuPont, S.T., Glover, J.D., Lal, R., Dungait, J.A.J., 2014. Soil organic carbon dynamics 75 years after land-use change in perennial grassland and annual wheat agricultural systems. Biogeochemistry 120, 37–49. https://doi.org/10.1007/s10533-014-9980-3

Bouraoui, F., Grizzetti, B., 2014. Modelling mitigation options to reduce diffuse nitrogen water pollution from agriculture. Science of The Total Environment 468–469, 1267–1277. https://doi.org/10.1016/j.scitotenv.2013.07.066

Bowley, P., 1996. Ontario Agriculture in the 1910s: The Move Toward Regional Specialization in Crop Production.

Bowley, P.M., 2013. A Century of Soybeans: Scientific Research and Mixed Farming in Agricultural Southern Ontario, 1881-1983. University of Guelph.

Boyer, E.W., Goodale, C.L., Jaworski, N.A., Howarth, R.W., 2002. Anthropogenic nitrogen sources and relationships to riverine nitrogen export in the northeastern U.S.A., in: Boyer, E.W., Howarth, R.W. (Eds.), The Nitrogen Cycle at Regional to Global Scales. Springer Netherlands, Dordrecht, pp. 137–169. https://doi.org/10.1007/978-94-017-3405-9_4

Carpenter, S.R., Caraco, N.F., Correll, D.L., Howarth, R.W., Sharpley, A.N., Smith, V.H., 1998. Nonpoint pollution of surface waters with phosphorus and nitrogen. Ecological applications 8, 559–568.

Chaffin, J.D., Mishra, S., Kane, D.D., Bade, D.L., Stanislawczyk, K., Slodysko, K.N., Jones, K.W., Parker, E.M., Fox, E.L., 2019. Cyanobacterial blooms in the central basin of Lake Erie:

Potentials for cyanotoxins and environmental drivers. Journal of Great Lakes Research 45, 277–289. https://doi.org/10.1016/j.jglr.2018.12.006

Chen, D., Shen, H., Hu, M., Wang, J., Zhang, Y., Dahlgren, R.A., 2018. Legacy Nutrient Dynamics at the Watershed Scale: Principles, Modeling, and Implications, in: Advances in Agronomy. Elsevier, pp. 237–313. https://doi.org/10.1016/bs.agron.2018.01.005

Choquette, A.F., Hirsch, R.M., Murphy, J.C., Johnson, L.T., Confesor, R.B., 2019. Tracking changes in nutrient delivery to western Lake Erie: Approaches to compensate for variability and trends in streamflow. Journal of Great Lakes Research 45, 21–39. https://doi.org/10.1016/j.jglr.2018.11.012

Cleveland, C.C., Liptzin, D., 2007. C:N:P stoichiometry in soil: is there a "Redfield ratio" for the microbial biomass? Biogeochemistry 85, 235–252. https://doi.org/10.1007/s10533-007-9132-0

Conley, D.J., Paerl, H.W., Howarth, R.W., Boesch, D.F., Seitzinger, S.P., Havens, K.E., Lancelot, C., Likens, G.E., 2009. ECOLOGY: Controlling Eutrophication: Nitrogen and Phosphorus. Science 323, 1014–1015. https://doi.org/10.1126/science.1167755

Davidson, E.A., Ackerman, I.L., 1993. Changes in soil carbon inventories following cultivation of previously untilled soils. Biogeochemistry 20, 161–193. https://doi.org/10.1007/BF00000786

Davis, C.C., 1964. Evidence for the Eutrophication of Lake Erie from Phytoplankton Records. Limnology and Oceanography 9, 275–283. https://doi.org/10.4319/lo.1964.9.3.0275

Di, H.J., Cameron, K.C., 2002. Nitrate leaching in temperate agroecosystems: sources, factors and mitigating strategies 21.

Dodds, W.K., 2006. Nutrients and the “dead zone”: the link between nutrient ratios and dissolved oxygen in the northern Gulf of Mexico. Frontiers in Ecology and the Environment 4, 211–217. https://doi.org/10.1890/1540-9295(2006)004[0211:NATDZT]2.0.CO;2

Dolan, D.M., 1993. Point Source Loadings of Phosphorus to Lake Erie: 1986–1990. Journal of Great Lakes Research 19, 212–223. https://doi.org/10.1016/S0380-1330(93)71212-5

Dorff, E., Beaulieu, M.S., 2014. Feeding the soil puts food on your plate (Analytical Paper), Canadian Agriculture at a Glance. Statistics Canada.

Dove, A., Chapra, S.C., 2015. Long-term trends of nutrients and trophic response variables for the Great Lakes: Great Lakes nutrient trends. Limnology and Oceanography 60, 696–721. https://doi.org/10.1002/lno.10055

Duinen, G.V., 2008. How a century of ammonia synthesis changed the world. nature geoscience 1, 4.

Elser, J.J., Bracken, M.E.S., Cleland, E.E., Gruner, D.S., Harpole, W.S., Hillebrand, H., Ngai, J.T., Seabloom, E.W., Shurin, J.B., Smith, J.E., 2007. Global analysis of nitrogen and phosphorus limitation of primary producers in freshwater, marine and terrestrial ecosystems. Ecology Letters 10, 1135–1142. https://doi.org/10.1111/j.1461-0248.2007.01113.x

Fastner, J., Abella, S., Litt, A., Morabito, G., Vörös, L., Pálffy, K., Straile, D., Kümmerlin, R., Matthews, D., Phillips, M.G., Chorus, I., 2016. Combating cyanobacterial proliferation by avoiding or treating inflows with high P load—experiences from eight case studies. Aquatic Ecology 50, 367–383. https://doi.org/10.1007/s10452-015-9558-8

Fee, E.J., 1979. A relation between lake morphometry and primary productivity and its use in interpreting whole-lake eutrophication experiments: Productivity of ELA lakes. Limnology and Oceanography 24, 401–416. https://doi.org/10.4319/lo.1979.24.3.0401

Foufoula-Georgiou, E., Takbiri, Z., Czuba, J.A., Schwenk, J., 2015. The change of nature and the nature of change in agricultural landscapes: Hydrologic regime shifts modulate ecological transitions: Hydrology modulates ecological transitions. Water Resources Research 51, 6649–6671. https://doi.org/10.1002/2015WR017637

G. R. Smith, P., 2015. Long-Term Temporal Trends in Agri-Environment and Agricultural Land Use in Ontario, Canada: Transformation, Transition and Significance. Journal of Geography and Geology 7. https://doi.org/10.5539/jgg.v7n2p32

Galloway, J.N., Schlesinger, W.H., Levy, H., Michaels, A., Schnoor, J.L., 1995. Nitrogen fixation: Anthropogenic enhancement-environmental response. Global Biogeochemical Cycles 9, 235–252. https://doi.org/10.1029/95GB00158

Gobler, C.J., Burkholder, J.M., Davis, T.W., Harke, M.J., Johengen, T., Stow, C.A., Van de Waal, D.B., 2016. The dual role of nitrogen supply in controlling the growth and toxicity of cyanobacterial blooms. Harmful Algae 54, 87–97. https://doi.org/10.1016/j.hal.2016.01.010

Grand River Conservation Authority, 2016. Wetlands.

Grand River Conservation Authority, 2014. Grand River Watershed Water Management Plan.

Grand River Conservation Authority, 2013. Water Quality Targets to Support Healthy and Resilient Aquatic Ecosystems in the Grand River Watershed, Grand River Water Management Plan. Cambridge, Ont.

Grand River Conservation Authority, 2008. Grand River Watershed Characterization Report. Grand River Conservation Authority.

Gupta, H.V., Kling, H., Yilmaz, K.K., Martinez, G.F., 2009. Decomposition of the mean squared error and NSE performance criteria: Implications for improving hydrological modelling. Journal of Hydrology 377, 80–91. https://doi.org/10.1016/j.jhydrol.2009.08.003

Haag, D., Kaupenjohann, M., 2001. Landscape fate of nitrate fluxes and emissions in Central Europe A critical review of concepts, data, and models for transport and retention 21.

Haejin Han, J. David Allan, 2008. Estimation of Nitrogen Inputs to Catchments: Comparison of Methods and Consequences for Riverine Export Prediction. Biogeochemistry 91, 177–199.

Hamilton, S.K., 2012. Biogeochemical time lags may delay responses of streams to ecological restoration: Time lags in stream restoration. Freshwater Biology 57, 43–57. https://doi.org/10.1111/j.1365-2427.2011.02685.x

Heisler, J., Glibert, P.M., Burkholder, J.M., Anderson, D.M., Cochlan, W., Dennison, W.C., Dortch, Q., Gobler, C.J., Heil, C.A., Humphries, E., Lewitus, A., Magnien, R., Marshall, H.G., Sellner, K., Stockwell, D.A., Stoecker, D.K., Suddleson, M., 2008. Eutrophication and harmful algal blooms: A scientific consensus. Harmful Algae 8, 3–13. https://doi.org/10.1016/j.hal.2008.08.006

Hember, R.A., 2018. Spatially and temporally continuous estimates of annual total nitrogen deposition over North America, 1860–2013. Data in Brief 17, 134–140. https://doi.org/10.1016/j.dib.2017.12.052

Hirsch, R., Cicco, L.A., 2015. Exploration and Graphics for RivEr Trends (EGRET).

Hirsch, R.M., Moyer, D.L., Archfield, S.A., 2010. Weighted Regressions on Time, Discharge, and Season (WRTDS), with an Application to Chesapeake Bay River Inputs1: Weighted Regressions on Time, Discharge, and Season (WRTDS), With an Application to Chesapeake Bay River Inputs. JAWRA Journal of the American Water Resources Association 46, 857–880. https://doi.org/10.1111/j.1752-1688.2010.00482.x

Ho, J.C., Stumpf, R.P., Bridgeman, T.B., Michalak, A.M., 2017. Using Landsat to extend the historical record of lacustrine phytoplankton blooms: A Lake Erie case study. Remote Sensing of Environment 191, 273–285. https://doi.org/10.1016/j.rse.2016.12.013

Hobbs, E.H., Muendel, H.-H., 1983. Water Requirements of Irrigated Soymeans in Southern Alberta. Canadian Journal of Plant Science 63, 855–860. https://doi.org/10.4141/cjps83-108

Hofmann, N., Beaulieu, M.S., Statistics Canada, Agriculture Division, 2006. A geographical profile of manure production in Canada, 2001. Statistics Canada, Agriculture Division, Ottawa, Ont.

Hong, B., Swaney, D.P., 2013. NANI Accounting Toolbox ,Version 3.1.0.

Hong, B., Swaney, D.P., Howarth, R.W., 2013. Estimating Net Anthropogenic Nitrogen Inputs to U.S. Watersheds: Comparison of Methodologies. Environmental Science & Technology 47, 5199–5207. https://doi.org/10.1021/es303437c

Hong, B., Swaney, D.P., Howarth, R.W., 2011. A toolbox for calculating net anthropogenic nitrogen inputs (NANI). Environmental Modelling & Software 26, 623–633. https://doi.org/10.1016/j.envsoft.2010.11.012

Hong, B., Swaney, D.P., McCrackin, M., Svanbäck, A., Humborg, C., Gustafsson, B., Yershova, A., Pakhomau, A., 2017. Advances in NANI and NAPI accounting for the Baltic drainage basin:

spatial and temporal trends and relationships to watershed TN and TP fluxes. Biogeochemistry 133, 245–261. https://doi.org/10.1007/s10533-017-0330-0

Hong, B., Swaney, D.P., Mörth, C.-M., Smedberg, E., Eriksson Hägg, H., Humborg, C., Howarth, R.W., Bouraoui, F., 2012. Evaluating regional variation of net anthropogenic nitrogen and phosphorus inputs (NANI/NAPI), major drivers, nutrient retention pattern and management implications in the multinational areas of Baltic Sea basin. Ecological Modelling 227, 117–135. https://doi.org/10.1016/j.ecolmodel.2011.12.002

Ilampooranan, I., Van Meter, K.J., Basu, N.B., 2019. A Race Against Time: Modeling Time Lags in Watershed Response. Water Resources Research 55, 3941–3959. https://doi.org/10.1029/2018WR023815

Iman, R.L., Conover, W.J., 1979. The Use of the Rank Transform in Regression. Technometrics 21, 499–509. https://doi.org/10.1080/00401706.1979.10489820

International Joint Commission, 1983. Great Lakes Water Quality Agreement of 1978 and Phosphorus Load Reduction Supplement.

International Joint Commission, 1970. Pollution of Lake Erie, Lake Ontario and the International Section of the St. Lawrence River 114.

International Joint Commission, 1965. Interim Report on the Pollution of Lake Erie, Lake Ontario and the International Section of the St. Lawrence River 22.

Janssen, B.H., 1984. A simple method for calculating decomposition and accumulation of 'young' soil organic matter, in: Tinsley, J., Darbyshire, J.F. (Eds.), Biological Processes and Soil Fertility. Springer Netherlands, Dordrecht, pp. 297–304. https://doi.org/10.1007/978-94-009-6101-2_26

Kaika, M., 2003. The Water Framework Directive: A New Directive for a Changing Social, Political and Economic European Framework. European Planning Studies 11, 299–316. https://doi.org/10.1080/09654310303640

Kellogg, R.L., Lander, C.H., Moffitt, D.C., Gollehon, N., 2000. Manure Nutrients Relative to the Capacity of Cropland and Pastureland to Assimilate Nutrients: Spatial and Temporal Trends for the United States. U.S. Department of Agriculture.

Kleinman, P., Sharpley, A., Buda, A., McDowell, R., Allen, A., 2011. Soil controls of phosphorus in runoff: Management barriers and opportunities. Canadian Journal of Soil Science 91, 329–338. https://doi.org/10.4141/cjss09106

Kronvang, B., Jeppesen, E., Conley, D.J., Søndergaard, M., Larsen, S.E., Ovesen, N.B., Carstensen, J., 2005. Nutrient pressures and ecological responses to nutrient loading reductions in Danish streams, lakes and coastal waters. Journal of Hydrology 304, 274–288. https://doi.org/10.1016/j.jhydrol.2004.07.035

Lassaletta, L., Billen, G., Grizzetti, B., Anglade, J., Garnier, J., 2014. 50 year trends in nitrogen use efficiency of world cropping systems: the relationship between yield and nitrogen input to cropland. Environmental Research Letters 9, 105011. https://doi.org/10.1088/1748-9326/9/10/105011

Lewis, W.M., Wurtsbaugh, W.A., 2008. Control of Lacustrine Phytoplankton by Nutrients: Erosion of the Phosphorus Paradigm. International Review of Hydrobiology 93, 446–465. https://doi.org/10.1002/iroh.200811065

Liu, Y., Engel, B.A., Flanagan, D.C., Gitau, M.W., McMillan, S.K., Chaubey, I., 2017. A review on effectiveness of best management practices in improving hydrology and water quality: Needs

and opportunities. Science of The Total Environment 601–602, 580–593. https://doi.org/10.1016/j.scitotenv.2017.05.212

Lloret, J., Valiela, I., 2016. Unprecedented decrease in deposition of nitrogen oxides over North America: the relative effects of emission controls and prevailing air-mass trajectories. Biogeochemistry 129, 165–180. https://doi.org/10.1007/s10533-016-0225-5

Loomer, H.A., Cooke, S.E., 2011. Water Quality in the Grand River Watershed: Current Conditions & Trends (2003 – 2008). Grand River Conservation Authority.

Maccoux, M.J., Dove, A., Backus, S.M., Dolan, D.M., 2016. Total and soluble reactive phosphorus loadings to Lake Erie. Journal of Great Lakes Research 42, 1151–1165. https://doi.org/10.1016/j.jglr.2016.08.005

Mackie, G.L., Rooke, J.B., Roff, J.C., Gerrath, J.F., 1983. Effects of changes in discharge level on temperature and oxygen regimes in a new reservoir and downstream. Hydrobiologia 101, 179–187. https://doi.org/10.1007/BF00009873

Matott, L.S., 2017. OSTRICH: an Optimization Software Tool, Documentation and User's Guide, Version 17.12.19.

McGuire, K.J., McDonnell, J.J., 2006. A review and evaluation of catchment transit time modeling. Journal of Hydrology 330, 543–563. https://doi.org/10.1016/j.jhydrol.2006.04.020

Meals, D.W., Dressing, S.A., Davenport, T.E., 2010. Lag Time in Water Quality Response to Best Management Practices: A Review. Journal of Environment Quality 39, 85. https://doi.org/10.2134/jeq2009.0108

Mekonnen, M.M., Hoekstra, A.Y., 2018. Global Anthropogenic Phosphorus Loads to Freshwater and Associated Grey Water Footprints and Water Pollution Levels: A High-Resolution Global

Study: GLOBAL ANTHROPOGENIC PHOSPHORUS LOADS. Water Resources Research 54, 345–358. https://doi.org/10.1002/2017WR020448

Ministry of Environment and Climate Change, 2016. Provincial Water Quality Monitoring Network.

Ministry of Environment, and Energy (MOE), 1994. Water Management Policies, Guidelines, Provincial Water Quality Objectives. Toronto, ON.

Mishra, S., 2009. Uncertainty and sensitivity analysis techniques for hydrologic modeling. Journal of Hydroinformatics 11, 282–296. https://doi.org/10.2166/hydro.2009.048

Mitchell, B., Shrubsole, D., 1992. Ontario Conservation Authorities: Myth and Reality, Department of Geography publication series. University of Waterloo, Department of Geography.

Muleta, M.K., Nicklow, J.W., 2005. Sensitivity and uncertainty analysis coupled with automatic calibration for a distributed watershed model. Journal of Hydrology 306, 127–145. https://doi.org/10.1016/j.jhydrol.2004.09.005

NAtChem, 1995. Summary Statistics of Precipitation Chemsitry Data.

National Hydrological Service, 2016. Canadian Hydrometric Data.

Oosterhuis, D.M., Scott, H.D., Hampton, R.E., Wullschleger, S.D., 1990. Physiological responses of two soybean [Glycine max (L.) Merr] cultivars to short-term flooding. Environmental and Experimental Botany 30, 85–92.

Paerl, H.W., Scott, J.T., McCarthy, M.J., Newell, S.E., Gardner, W.S., Havens, K.E., Hoffman, D.K., Wilhelm, S.W., Wurtsbaugh, W.A., 2016. It Takes Two to Tango: When and Where Dual Nutrient (N & P) Reductions Are Needed to Protect Lakes and Downstream Ecosystems. Environmental Science & Technology 50, 10805–10813. https://doi.org/10.1021/acs.est.6b02575

Paerl, H.W., Xu, H., McCarthy, M.J., Zhu, G., Qin, B., Li, Y., Gardner, W.S., 2011. Controlling harmful cyanobacterial blooms in a hyper-eutrophic lake (Lake Taihu, China): The need for a dual nutrient (N & P) management strategy. Water Research 45, 1973–1983. https://doi.org/10.1016/j.watres.2010.09.018

Parris, K., 1998. Agricultural nutrient balances as agri-environmental indicators: an OECD perspective. Environmental Pollution 102, 219–225.

Ramankutty, N., Foley, J.A., 2007. Historic Croplands Dataset.

Ramankutty, N., Foley, J.A., 1999. Estimating historical changes in global land cover: Croplands from 1700 to 1992. Global Biogeochemical Cycles 13, 997–1027. https://doi.org/10.1029/1999GB900046

Richards, R.P., Baker, D.B., Eckert, D.J., 2002. Trends in Agriculture in the LEASEQ Watersheds, 1975-1995. Journal of Environmental Quality 31, 17–24. https://doi.org/10.2134/jeq2002.1700

Ruddy, B.C., Lorenz, D.L., Mueller, D.K., 2006. County-Level Estimates of Nutrient Inputs to the Land Surface of the Conterminous United States, 1982–2001, Scientific Investigations Report. USGS.

Schilling, K.E., Spooner, J., 2006. Effects of Watershed-Scale Land Use Change on Stream Nitrate Concentrations. Journal of Environmental Quality 35, 2132–2145. https://doi.org/10.2134/jeq2006.0157

Schindler, D.W., 1974. Eutrophication and Recovery in Experimental Lakes: Implications for Lake Management. Science, New Series 184, 897–899.

Schindler, D.W., Carpenter, S.R., Chapra, S.C., Hecky, R.E., Orihel, D.M., 2016. Reducing Phosphorus to Curb Lake Eutrophication is a Success. Environmental Science & Technology 50, 8923–8929. https://doi.org/10.1021/acs.est.6b02204

Sebilo, M., Mayer, B., Nicolardot, B., Pinay, G., Mariotti, A., 2013. Long-term fate of nitrate fertilizer in agricultural soils. Proceedings of the National Academy of Sciences 110, 18185–18189. https://doi.org/10.1073/pnas.1305372110

Sharpley, A.N., Kleinman, P.J.A., Jordan, P., Bergström, L., Allen, A.L., 2009. Evaluating the Success of Phosphorus Management from Field to Watershed. Journal of Environmental Quality 38, 1981–1988. https://doi.org/10.2134/jeq2008.0056

Six, J., Conant, R.T., Paul, E.A., Paustian, K., 2002. Stabilization mechanisms of soil organic matter: Implications for C-saturation of soils 22.

Smil, V., 1999. Nitrogen in crop production: An account of global flows. Global Biogeochemical Cycles 13, 647–662. https://doi.org/10.1029/1999GB900015

Smith, R.B., Bass, B., Sawyer, D., Depew, D., Watson, S.B., 2019. Estimating the economic costs of algal blooms in the Canadian Lake Erie Basin. Harmful Algae 87, 101624. https://doi.org/10.1016/j.hal.2019.101624

Smolders, A.J.P., Lucassen, E.C.H.E.T., Bobbink, R., Roelofs, J.G.M., Lamers, L.P.M., 2010. How nitrate leaching from agricultural lands provokes phosphate eutrophication in groundwater fed wetlands: the sulphur bridge. Biogeochemistry 98, 1–7. https://doi.org/10.1007/s10533-009-9387-8

Spoelstra, J., Schiff, S.L., Elgood, R.J., Semkin, R.G., Jeffries, D.S., 2001. Tracing the Sources of Exported Nitrate in the Turkey Lakes Watershed Using 15 N/ 14 N and 18 O/ 16 O isotopic ratios. Ecosystems 4, 536–544. https://doi.org/10.1007/s10021-001-0027-y

Sprague, L.A., Gronberg, J.A.M., 2012. Relating Management Practices and Nutrient Export in Agricultural Watersheds of the United States. Journal of Environment Quality 41, 1939. https://doi.org/10.2134/jeq2012.0073

Statistics Canada, 2017. Table 32-10-0359-01: Estimated areas, yield, production, average farm price and total farm value of principal field crops, in metric and imperial units.

Statistics Canada, 2016a. Canadian Census of Agriculture.

Statistics Canada, 2016b. Table 32-10-0039-01 Fertilizer shipments to Canadian agriculture markets, by nutrient content and fertilizer year, cumulative data.

Statistics Canada, 2016c. Canadian Census of Population.

Tesoriero, A.J., Duff, J.H., Wolock, D.M., Spahr, N.E., Almendinger, J.E., 2009. Identifying Pathways and Processes Affecting Nitrate and Orthophosphate Inputs to Streams in Agricultural Watersheds. Journal of Environmental Quality 38, 1892–1900. https://doi.org/10.2134/jeq2008.0484

Tolson, B.A., Shoemaker, C.A., 2007. Dynamically dimensioned search algorithm for computationally efficient watershed model calibration: DYNAMICALLY DIMENSIONED SEARCH ALGORITHM. Water Resources Research 43. https://doi.org/10.1029/2005WR004723

Turner, R.E., Rabalais, N.N., Justic, D., 2008. Gulf of Mexico Hypoxia: Alternate States and a Legacy. Environmental Science & Technology 42, 2323–2327. https://doi.org/10.1021/es071617k

Van Meter, K.J., Basu, N.B., 2017. Time lags in watershed-scale nutrient transport: an exploration of dominant controls. Environmental Research Letters 12, 084017. https://doi.org/10.1088/1748-9326/aa7bf4

Van Meter, K.J., Basu, N.B., 2015. Catchment Legacies and Time Lags: A Parsimonious Watershed Model to Predict the Effects of Legacy Storage on Nitrogen Export. PLOS ONE 10, e0125971. https://doi.org/10.1371/journal.pone.0125971

Van Meter, K.J., Basu, N.B., Van Cappellen, P., 2017. Two centuries of nitrogen dynamics: Legacy sources and sinks in the Mississippi and Susquehanna River Basins: Two centuries of nitrogen dynamics. Global Biogeochemical Cycles 31, 2–23. https://doi.org/10.1002/2016GB005498

Van Meter, K.J., Basu, N.B., Veenstra, J.J., Burras, C.L., 2016. The nitrogen legacy: emerging evidence of nitrogen accumulation in anthropogenic landscapes. Environmental Research Letters 11, 035014. https://doi.org/10.1088/1748-9326/11/3/035014

Van Meter, K.J., Van Cappellen, P., Basu, N.B., 2018. Legacy nitrogen may prevent achievement of water quality goals in the Gulf of Mexico. Science eaar4462. https://doi.org/10.1126/science.aar4462

Watson, S.B., Miller, C., Arhonditsis, G., Boyer, G.L., Carmichael, W., Charlton, M.N., Confesor, R., Depew, D.C., Höök, T.O., Ludsin, S.A., Matisoff, G., McElmurry, S.P., Murray, M.W., Peter Richards, R., Rao, Y.R., Steffen, M.M., Wilhelm, S.W., 2016. The re-eutrophication

of Lake Erie: Harmful algal blooms and hypoxia. Harmful Algae 56, 44–66. https://doi.org/10.1016/j.hal.2016.04.010

Wheaton, E., Kulshreshtha, S., Wittrock, V., Koshida, G., 2008. Dry times: hard lessons from the Canadian drought of 2001 and 2002: Dry times. The Canadian Geographer / Le Géographe canadien 52, 241–262. https://doi.org/10.1111/j.1541-0064.2008.00211.x

Whitmore, A.P., Bradbury, N.J., Johnson, P.A., 1992. Potential contribution of ploughed grassland to nitrate leaching. Agriculture, Ecosystems & Environment 39, 221–233. https://doi.org/10.1016/0167-8809(92)90056-H

Worrall, F., Spencer, E., Burt, T.P., 2009. The effectiveness of nitrate vulnerable zones for limiting surface water nitrate concentrations. Journal of Hydrology 370, 21–28. https://doi.org/10.1016/j.jhydrol.2009.02.036

Zbieranowski, A.L., Aherne, J., 2011. Long-term trends in atmospheric reactive nitrogen across Canada: 1988–2007. Atmospheric Environment 45, 5853–5862. https://doi.org/10.1016/j.atmosenv.2011.06.080

Zhang, X., 2016. Spatio-Temporal Patterns in Net Anthropogenic Nitrogen and Phosphorus Inputs Across the Grand River Watershed. University of Waterloo, Waterloo, Ontario.

Appendix A Parameter Ranges for Sensivity Analysis

Parameter	Lower bound	Upper bound	Reference
M_s	4000	12000	Zinke et al., 1998
k_a	0.09	0.17	Van Meter et al., 2017
λ	0.25	0.75	Van Meter et al., 2017
h_c	0.14	0.26	Van Meter et al., 2017
h_{nc}	0.28	0.75	Van Meter et al., 2017
μ	3	27	Van Meter et al., 2017
γ	0.07	0.13	Van Meter et al., 2017
k_h	0.56	1	(Van Meter et al., 2017)

Appendix B Land Cover Transition (LCT) Year in all subbasins

	soy exceed Hay + small grains	corn exceed Hay + Small Grains	Row crops exceeding Small grains
Canagagigue Creek	Never	2001	1975
Conestogo River	Never	Never	1990
Whitemans Creek	1998	1970	1967
Nith, New Hamburg	Never	1981	1974
Nith, Canning	Never	1975	1972
Eramosa River	1999	1979	1989
Speed, Armstrong	2014	2002	1990
Speed, Guelph	2002	1998	1990
Grand, Marsville	2016	Never	1998
Grand, Shand Dam	2016	Never	1998
Grand, West Montrose	2017	Never	1994
Grand, Galt	2016	2011	1989
Grand, Brantford	2016	1979	1975
Grand, York	2013	1977	1975

Appendix C Best run parameter values for all subbasins

Parameter	Description	Canagagigue Creek	Conestogo River	Whitemans Creek	Nith, New Hamburg	Nith, Canning	Eramosa River	Speed, Armstrong
M_s	Initial Nitrogen content in soil (kg/ha)	8632	7918	8517	8088	7947	7928	7752
k_a	Mineralization rate of active pool (yr^{-1})	0.13	0.16	0.16	0.14	0.15	0.14	0.12
λ	denitrification rate constant (soil) (yr^{-1})	0.25	0.25	0.25	0.25	0.25	0.42	0.27
h_c	cultivated humification coefficient	0.14	0.14	0.24	0.14	0.17	0.17	0.19
h_{nc}	non-cultivated humification coefficient	0.28	0.63	0.35	0.56	0.60	0.38	0.64
μ	mean travel time (yrs)	5.9	5.8	6.20	9.7	11.2	30.8	29.2
γ	denitrification rate constant (groundwater) (yr^{-1})	0.07	0.07	0.07	0.07	0.07	0.11	0.13
k_h	denitrification rate constant (wastewater) (yr^{-1})	0.63	0.85	0.84	0.85	0.85	0.83	0.85

Parameter	Description	Speed, Guelph	Grand, Marsville	Grand, Shand Dam	Grand, West Montrose	Grand, Galt	Grand, Brantford	Grand, York
M_s	Initial Nitrogen content in soil (kg/ha)	7950	8750	8125	8592	8274	8146	7498
k_a	Mineralization rate of active pool (yr^{-1})	0.17	0.09	0.09	0.11	0.09	0.14	0.09
λ	denitrification rate constant (soil) (yr^{-1})	0.36	0.25	0.36	0.25	0.32	0.25	0.25
h_c	cultivated humification coefficient	0.17	0.26	0.21	0.23	0.23	0.16	0.14
h_{nc}	non-cultivated humification coefficient	0.64	0.37	0.67	0.35	0.44	0.42	0.32
μ	mean travel time (yrs)	24.4	23.27	14.80	11.79	5.14	10.52	9.43
γ	denitrification rate constant (groundwater) (yr^{-1})	0.12	0.07	0.10	0.07	0.11	0.07	0.07
k_h	denitrification rate constant (wastewater) (yr^{-1})	0.85	0.85	0.85	0.84	0.77	0.84	0.80